Correlation of Graphene Defect Density in Saccharide Carbon Dots for Electrochemical Dopamine Detection

by

Ram Chandra Nepal

A Thesis Submitted in Partial Fulfilment of the Requirements for the Degree of

Master of Science in Chemistry

Middle Tennessee State University

April 2024

Thesis committee

Dr. Charles C. Chusuei, Major professor
Dr. Keying Ding
Dr. Chengshan Wang

ABSTRACT

A study was conducted to investigate the detection of dopamine levels in urine for the diagnosis of neuroblastoma, a childhood cancer. A series of carbon dots (sucrose, palatinose and raffinose) were synthesized in the Leblanc lab at U. Miami-Coral Gables and applied for the electrochemical sensing of dopamine. A cobalt oxide-sucrose carbon dot (Co_3O_4-SucCD) composite was developed, utilizing a 1:1 mixture (by mass) suspended in absolute anhydrous ethanol, followed by sonication for 30 min. to facilitate the tethering of sucrose carbon dots (SucCDs) onto the Co_3O_4 nanoparticles. The electrode demonstrated selectivity towards urea, uric acid, glucose, and ascorbic acid, common interferes in urine. With a limit of detection of 1.91 µM in PBS, the electrode exhibited a linear dynamic range of 10-100 µM, R^2=0.990, and successfully detected 5 µM dopamine in urine samples, suitable for identifying elevated dopamine levels indicative of neuroblastoma. Calibration curve fitting in simulated urine yielded a quadratic equation with an R^2 = 0.997. The diffusion coefficient of the electrode in phosphate buffer was determined to be 5.21 x 10^{-5} $cm^2 \cdot sec^{-1}$. The correlation between graphene defect density within the saccharide carbon dots for dopamine sensing was investigated, revealing that the defect density decreased in the order of SucCDs (0.195) > PalCDs (0.115) > RafCDs (0.0975), while the electrocatalytic sensitivity followed the trend of RafCDs < PalCDs < SucCDs. The composite particles exhibit an average size of 68.47 ± 0.77 nm with a coefficient of determination R^2= 0.978. SEM-EDX analysis indicates a presence of 0.6% cobalt within the composite. The data suggests that a multilayer of carbon dots (CDs) surrounds the cobalt oxide particles, rendering low atomic % cobalt as detected by EDX.

ACKNOWLEDGEMENT

I wish to express profound gratitude to Professor Charles C. Chusuei, my research mentor during my MS program at MTSU. His invaluable support and unmatched guidance have been instrumental in my success. I am grateful to be one of Dr. Chusuei's students. I also extend my sincere thanks to my graduate committee members, Dr. Chengshan Wang and Dr. Keying Ding, for their insightful advice and invaluable suggestions throughout my Master's program.

Special thanks go to Dr. Beng G Ooi, Dr. Ngee Sing Chong, and their student Biliquis Bintinlaiye for guiding me in obtaining Raman spectra for my samples. I appreciate Christopher J Clark, a doctoral scholar for his pivotal support to train me for the experimental part of my research. I would like to thank my current lab mate Matt Rollins for his continue support. I am thankful to Oscar Karki and his wife Rojita Panta for connecting me with MTSU. I express my sincere thanks to the Department of Chemistry at MTSU for providing me the opportunity to pursue my master’s degree, along with access to chemicals, research labs, materials, and instruments for my experiments. I am grateful to the Ms. Joyce Miller for SEM images and EDX data.

My deepest thanks, love, and respect go to my parents, Radha Devi Nepal and Krishna Prasad Nepal, for their continued support. I also want to mention my beloved wife, Hema Laxmi Nepal, and the joys of my heart, my twin babies, Himani Nepal, and Swornim Nepal, who have consistently motivated and supported me throughout life's journeys.

TABLE OF CONTENTS

Page

LIST OF FIGURES……Page

LIST OF TABLES

LIST OF FLOW CHARTS

Chapter 1

INTRODUCTION

Carbon is the first member of group IV (A) element which exist in different allotropic states. Carbon has four electrons in valence shell and can form four covalent bonds. This property of carbon gives rise to the excellent catenation ability. Carbon exists in distinct solid state allotropes with diverse structures and properties ranging from sp^3 hybridized diamond to sp^2 hybridized graphite. Carbon-based materials have played crucial roles in advancing material science. From traditional types like activated carbon and carbon black to newer varieties such as carbon fibres, graphite, graphene, and carbon nanotubes (CNTs), these materials have been central in diverse fields due to their environmental advantages. However, conventional macroscopic carbon materials lack the necessary band gap, limiting their effectiveness as fluorescent materials [1].

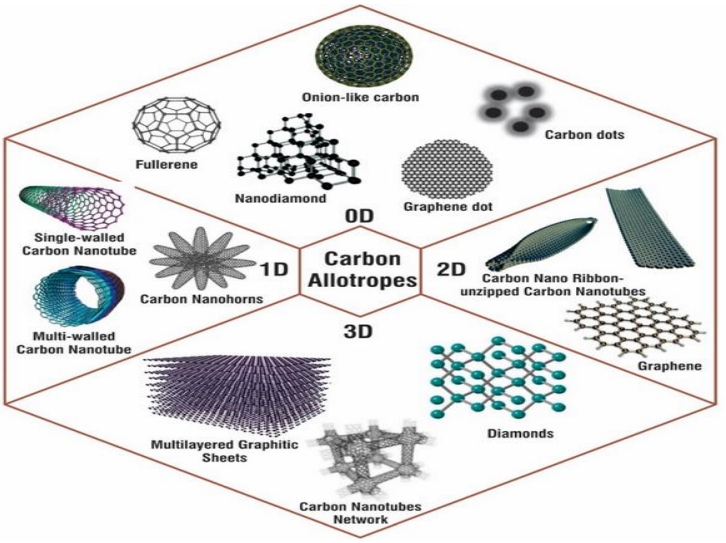

Fig 1. Various Nano forms of carbon allotropes with examples for 0D, 1D, 2D, and 3D carbon nanostructure. Reprinted with permission from Gaur et al., *Materials*, *14*(20), 5978 (open access).

Graphene defects and its major types

In three-dimensional crystals, defects are intrinsic when they disrupt the crystal's order naturally, without involving foreign atoms. On the other hand, impurities, which are foreign atoms, represent extrinsic defects [3]. In the Zero dimensional carbon nanoparticles, the point defects are found. Typically vacancies or interstitial atoms are introduced on the carbon dots. In one and two dimensional carbon nanomaterial such as graphene, and carbon nanotube, typically defects are tilted boundaries that divide two areas of these materials with different patterns, with the tilt axis perpendicular to the plane. These defects can be seen as a line where point defects have been rearranged.

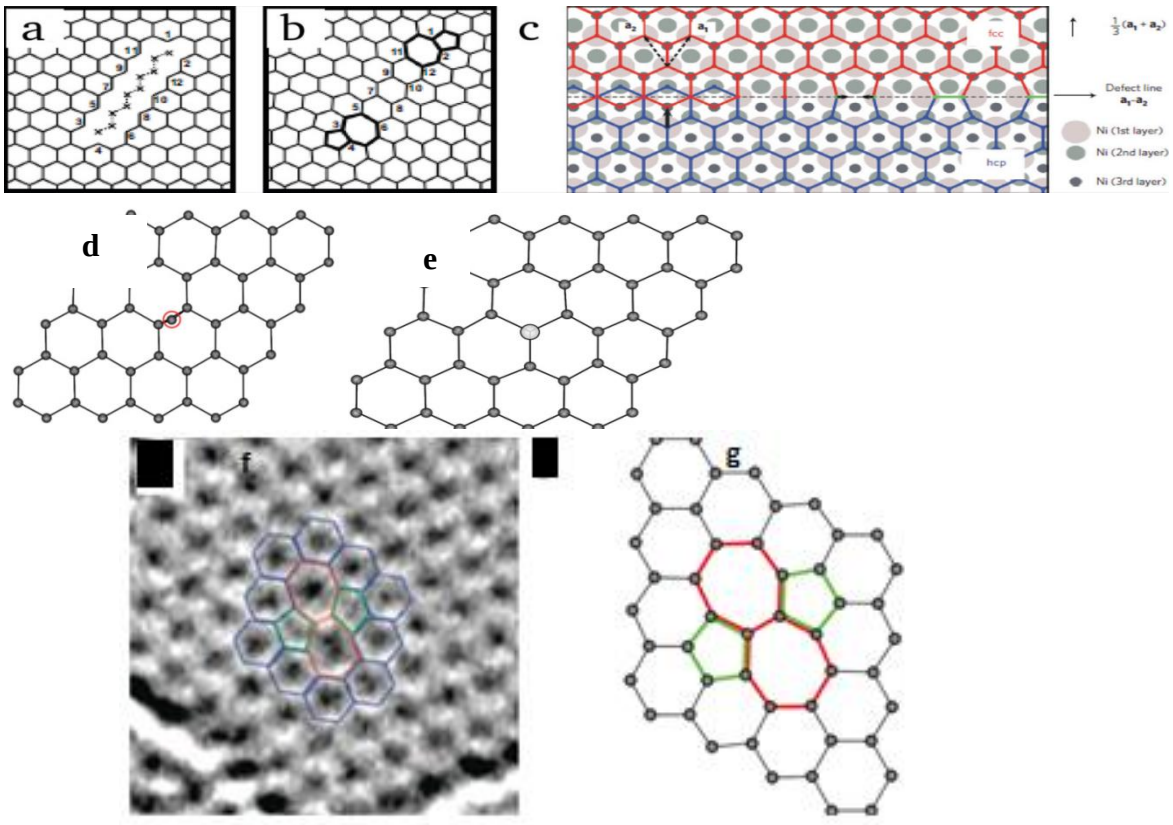

Fig 2. (a,b) Line defect formation from aligned vacancy structures; (c) grain boundary defect structure consisting of pentagon-pairs and octagons in graphene grown on a Ni substrate; (d, e) carbon adatoms: (d) single adatom in the bridge; typical atomic configurations of transition metal atoms adsorbed on single and double vacancies in a graphene sheet: (e) top viewj; (f, j) Stone–Wales defect SW, formed by rotating a carbon–carbon bond by 90°. Adapted with permission from Banhart et al., *ACS Nano* 5, no. 1 (January 25, 2011): 26–41. Copyright 2011, American Chemical Society.

Raman spectroscopy

Raman spectroscopy is a vibrational spectroscopy technique used for assessing molecular motion and fingerprinting species. Spectral information in Raman spectroscopy originates from the inelastic scattering of a monochromatic excitation source, namely the laser emitting at either 532 nm or 785 nm. This technique is useful to analyse gas, liquid or solid samples and needs almost no sample preparation.

Working principle of Raman Spectroscopy

When laser hits the particles, which are excited into the virtual excitation level by the absorption of energy of the laser. Then the particle returns to the lower energy level by emitting the energy. Inelastic collision between the photon and small particle like atom, and molecules are responsible for Raman scattering. It's about 1 in one million collisions in are inelastic collisions. If the energy of the scattered photon is lower than the incident photon, it is called Stokes shift or redshift because the wavelength of the scattered photon is longer than that of the incident photon.

If the energy of the scatter photon is higher than the incident photon, it is called the anti-stokes shift or blue shift because the wavelength of the scatter photon is shorter than that of the incident photon. It is a rare case because there are an insignificant number of particles in an excited state at normal temperature. Raman spectroscopy is crucially important in diverse fields of science including drug analysis [4], food analysis [5], textile analysis, polymer analysis [6], material science, and cell biology [7]. Since it is non-destructive, it is excessively used in forensic analysis [8].

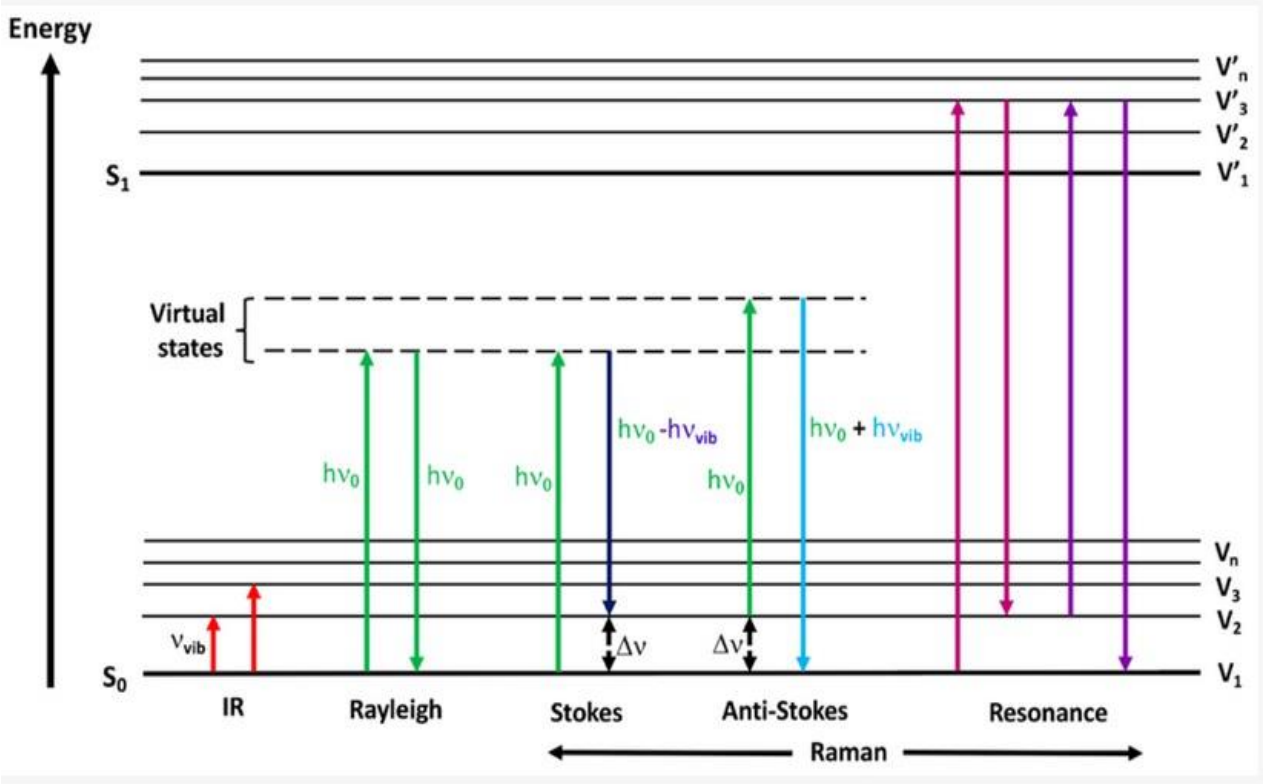

Fig 3. Jablonski energy diagram showing the transitions involved absorption, Rayleigh, Raman Stokes, anti-Stokes, and resonance Raman scattering as reported by Geraldes reprinted with the permission of ref [9]. (Open access)

Raman technique for defect quantification

Raman spectroscopy shows the distinct vibrational signature of a sample, enabling the extraction of valuable details about its chemical, structural physical characteristics. Raman spectroscopy can quantify Defects. Here, defects are quantified as peak area of D-band (1360 cm^{-1}) and pure graphene is quantified as G- band (1585 cm^{-1} respectively [10]. The D band represents sp^3 hybridization, indicative of disorder within the graphene sheet, whereas the G band signifies sp^2 hybridization, reflecting the orderly arrangement of carbon atoms in grapheme [11] The sp^2 carbon bonds result in highly polarisable π bonds which give an intense Raman signal. This is because the vibrational mode is Raman active and this occurs when the molecular polarisability changes during the vibration. The G-band,

located around 1585 cm^{-1}, corresponds to the in-plane stretching vibrations of sp^2-bonded carbon atoms. The position of this band is influenced by the number of layers present. The defect density is calculated as the ratio of intensity of D band to G band (I_D/I_G).

Rationale for using carbon dots instead of carbon nanotubes and graphene

The comprehensive study of D band is done to characterize lattice defects in carbon materials, both qualitatively and quantitatively [9, 12, and 13]. However, the presence of a D band doesn't always accurately represent topological defects and can be prone to misinterpretation [14]. In 2010 Gupta *etal*. reported that the presence of curvature on a graphene sheet can induce a small D band [15]. Carbon nanotubes, when exceeding a critical diameter, undergo spontaneous collapse into flattened structures [15]. Raman spectra analysis of both flattened and cylindrical carbon nanotubes reveals a distinctive and intense D band, even in the absence of lattice disorder [15]. The collapse induces this D band through curvature changes near edge cavities, despite overall framework continuity [16].

Conversely, CDs are less susceptible to curvature change and the intensity of D band is the exclusive indicator of defect quantity within the graphene sheet. The D band in the spectra is an artefact of change in the graphene curvature.

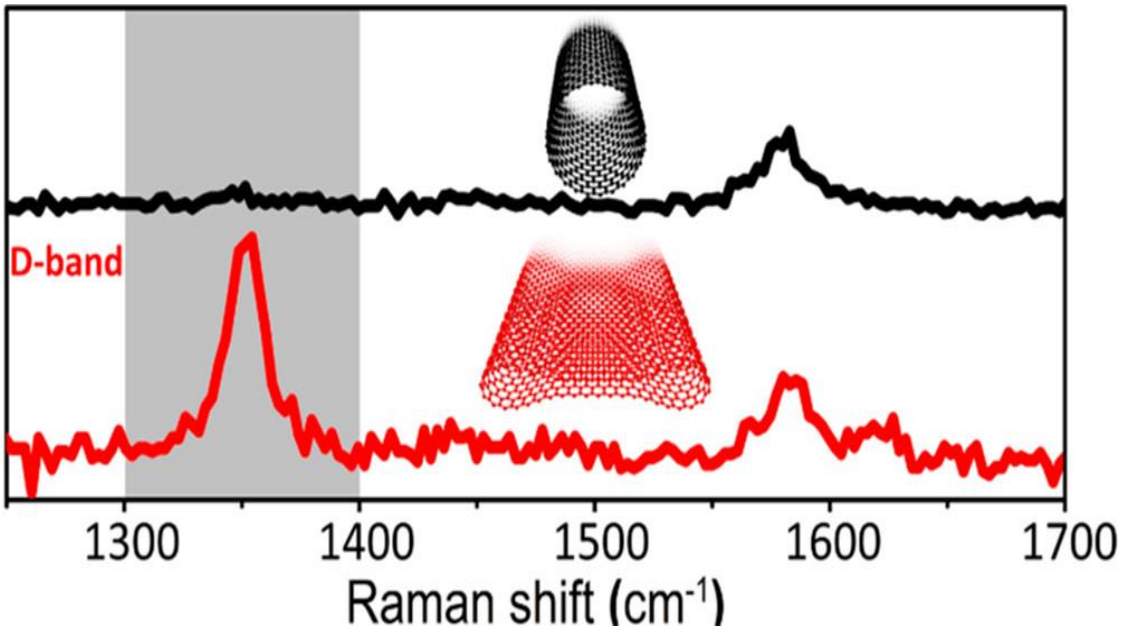

Fig 4. Removal of the inner CNT walls, flattening provokes an intense and narrow Raman D band Reprinted with permission from Peachu et al, *ACS Nano* 15, no. 1 (January 26, 2021): 596–603. Copyright 2021, American Chemical Society.

Carbon dots

Carbon dots (CDots) are zero dimensional particles supposed to have spherical shape particles smaller than 10 nm, initially discovered in 2004 during the purification of single-wall nanotubes [17]. They've since been extensively studied and used in various fields like energy conversion and storage [18], bio-imaging [19], drug delivery [20], metal sensor [21], and molecular ink [22].

Carbon dots are made mainly from carbon sources with nitrogen, sulphur doping, they're non-toxic unlike other nanoparticles like semiconductor quantum dots. CDs boast excellent photo stability and high fluorescence, comparable to quantum dots, making them great for bio-imaging. Unlike quantum dots, CDs' synthesis easier and cheaper, making them attractive for commercial applications like biomarkers, sensors, and even potential drug delivery systems. Understanding CDs optical properties at a molecular level is crucial for

their optimal use. Despite different starting materials, CDs exhibit similar photo physical behaviour formed under high temperature and pressure, urging further exploration into their physical and optical traits. Due to their biocompatible nature and simple production methods, CDs have become the focal point of extensive research. Subsequently, their photophysical characteristics were found to be comparable to semiconductor-based quantum dots. CDs exhibit superior optical qualities, including features like two-photon imaging, excitation-dependent photoluminescence emission, size-related photoluminescence emission, and resistance to photo bleaching. While some of these traits are unique to CDs, they are not exclusive to quantum dots. Beyond their advantageous optical attributes, CDs demonstrate cellular biocompatibility and offer versatility for various surface modifications. Carbon Dots are excellent electrode material since has tuneable band gap. It can be used to prepare composite material with other metal or metal oxide nanoparticle.

Synthesis of CDs

Generally, the synthesis procedures of the CDs are of two types: top-down and bottom-up synthetic approaches [23]. In the Top-down methods, the large carbon molecules are broken into smaller carbonic parts by applying external source of energy such as arc discharge, laser, etc. The initial top-down approach involved using arc-discharge on candle soot to create single-walled carbon nanotubes (SWCNTs) and accidently CDs were produced. Bottom-up methods are chemical approaches, which use carbon precursors to synthesize CDs. Bottom-up methods use lower cost starting materials and experimental apparatus, and the experimental ratio and conditions are easier to control than top-down

methods. Saccharides CDs for this research were synthesised by Elif Seven at University of Miami Coral Gables.

Hydrothermal production of CDs

Hydrothermal synthesis used 18 MΩ distilled water as the solvent, is commonly employed to produce highly crystalline nanoparticles in powder form. Similar to solvothermal synthesis, a mixture of precursors is introduced into a stainless-steel autoclave lined with Teflon. Optimal adjustments of temperature, reaction duration, and pressure conditions play a crucial role in controlling precursor solubility in water [24], as well as ensuring the homogeneity and crystallinity of the generated nanoparticles [25, 26]. Conducting hydrothermal synthesis at temperatures below 300 °C leads to substrate dehydration and polymerization, resulting in the development of diverse surface functionalities [27].

Advantage of hydrothermal synthesis of CDs

Hydrothermal synthesis predominantly employs water as a solvent, rendering it environmentally sustainable. Its cost-effectiveness stems from the versatility of available precursors and the absence of necessity for specialized, expensive instrumentation. Furthermore, it enables precise control over size, morphology, and surface functionalities of the synthesized materials.

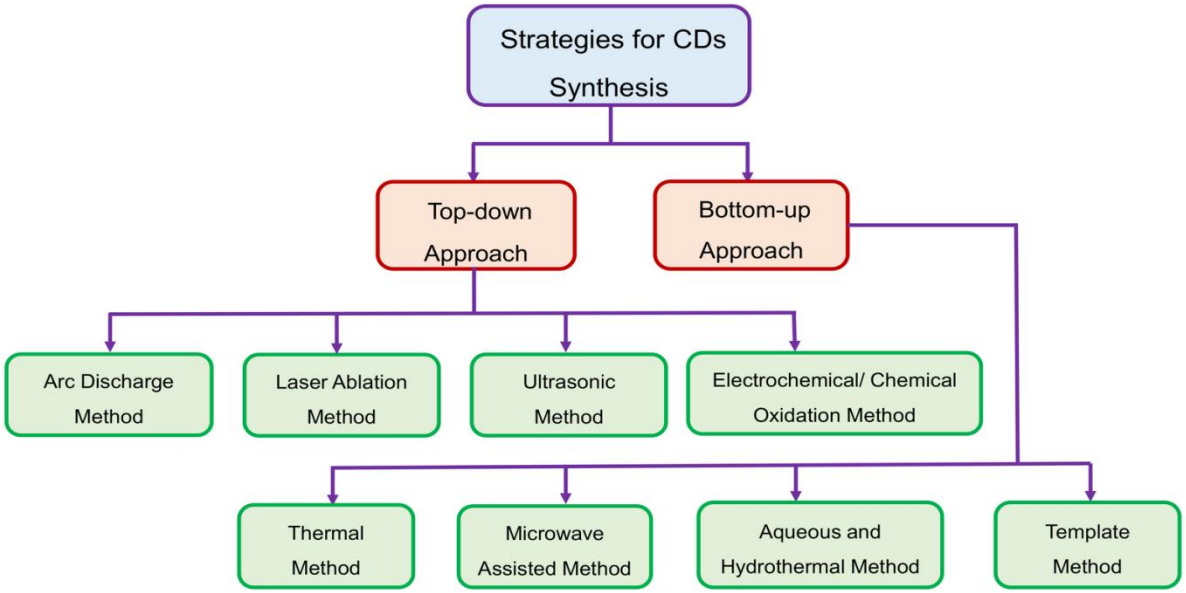

Fig 5. Different pathway to the preparation of CDs [28] reprinted from the *Nanomaterials 2021, 11, 252* (open access).

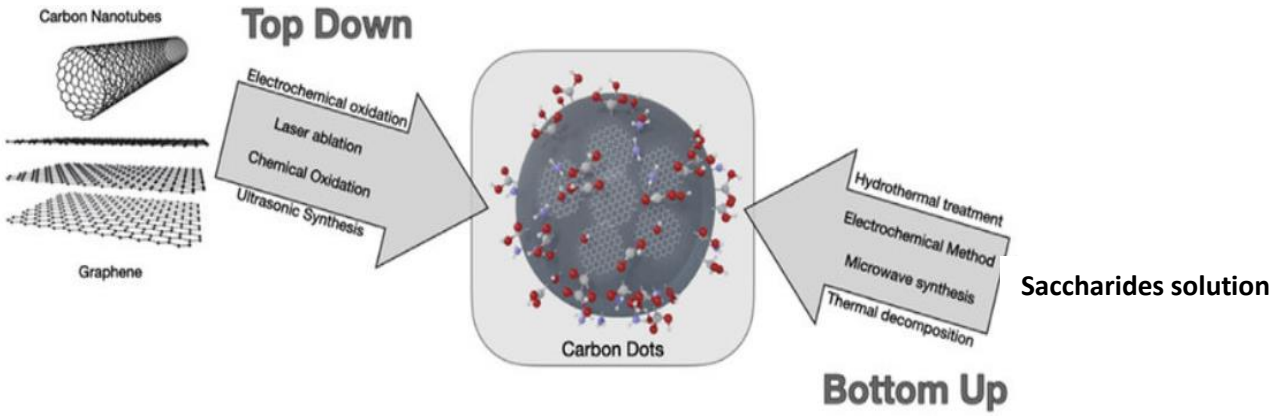

Fig 6. Experimental pathways of formation of CD [29]. Adapted with the permission of *Journal of Food and Drug Analysis* 28, no. 4 (December 2, 2020): 678–96.

Versatile applications of Carbon Dots

Electrochemical biosensors are able to directly transform intangible biological data into measurable electrical signals. Quantum confinement effect, surface state, edge defect, multi-emissive centres, heteroatom doping, and tuneable band gap between (HOMO) and

(LUMO) are responsible for their broad-spectrum properties of CDs. Biosensors have played important roles in various fields such as biomedicine, [30] agriculture, [31] food safety, [32] environmental, [33] and industrial monitoring [34-35].

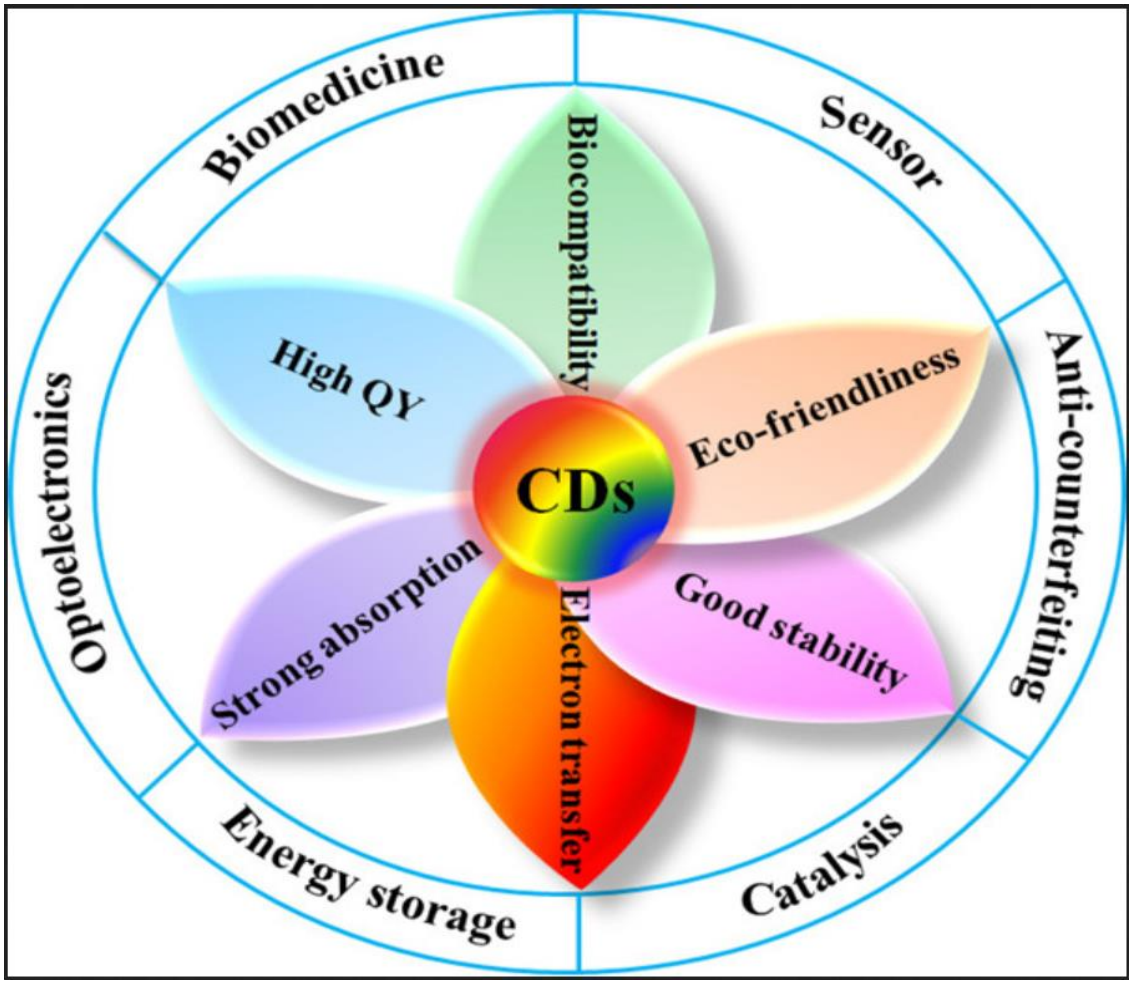

Fig 7. Versatile use of CDs. Reprinted with permission from Liu et al., *ACS Cent. Sci.* 2020, 6, 12, 2179-2195 American Chemical Society. Copyright 2020, American Chemical Society.

Dopamine and its quantitative analysis

Dopamine is well known neurotransmitters which has significance role to coordinate essential activities of the entire human system such as learning behaviour, emotion, and movements. The concentration of DA in human body and serum samples are found to be in

the nanomolar range. But the person suffering from neuroblastoma has elevated dopamine level up to micro molar range in urine. An imbalance of DA levels is associated with chronic diseases including Parkinson's disease, dementia, epilepsy, schizophrenia [37], and, neuroblastoma [38].

Neuroblastoma originates from sympathetic nervous tissue and it leads to the generation of significant quantities of catecholamine and their metabolites, which are excreted from the body through urine [39]. Dopamine in our body fluid and urine is present in association with ascorbic acid, uric acid, urea, glucose and ammonium salt. Fluorescence analysis [40, 41] and ultrahigh-performance liquid chromatography-electrospray ionization-tandem mass spectrometric methods (UHPLC/ESI-Q-TOF-MS) [42, 43] are employed to detect the DA level in urine and body fluid now days. The above-mentioned techniques are very expensive and need special knowledge to operate. On the other hand, an electrochemical method had more than 42 k publications after 2019 according to Sci Finder. This technique is easy, cost-effective, and real-time analysis.

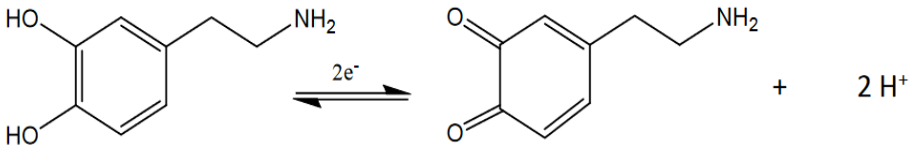

dopamine
(reduced species)

dopamine-o-quinone
(oxidized species)

Reversible redox reaction of dopamine

When the sweeping potential increases, the dopamine molecule oxidises to orthoquinone form and again changes into the original compound by the reduction process. The loss of electrons is oxidation**.**

Cyclic voltammetry and its working principle

Cyclic voltammetry (CV) is a powerful and popular electrochemical technique frequently employed to monitor the redox phenomenon of molecular species. The current has been measured as a function of potential. The experiment is done in three-electrode system electrochemical cell using: working electrode (WE), reference electrode (RE) and counter electrode (CE). The working electrode is selected based on analytes, where the potential is continually changed at a certain sweep rate. Working electrodes provide the surface for redox reactions. The reference electrode balances the potential with the working electrode. Generally, we have standard Ag/AgCl electrodes for reference electrode. Counter electrode balances the current on the working electrode makes a complete circuit and maintains constant interfacial potential. The working electrode acts as an anode when the potential increases and acts as a cathode to decrease the potential. On increasing the potential, oxidation occurs in the working electrode and on decreasing the potential, reduction takes place.

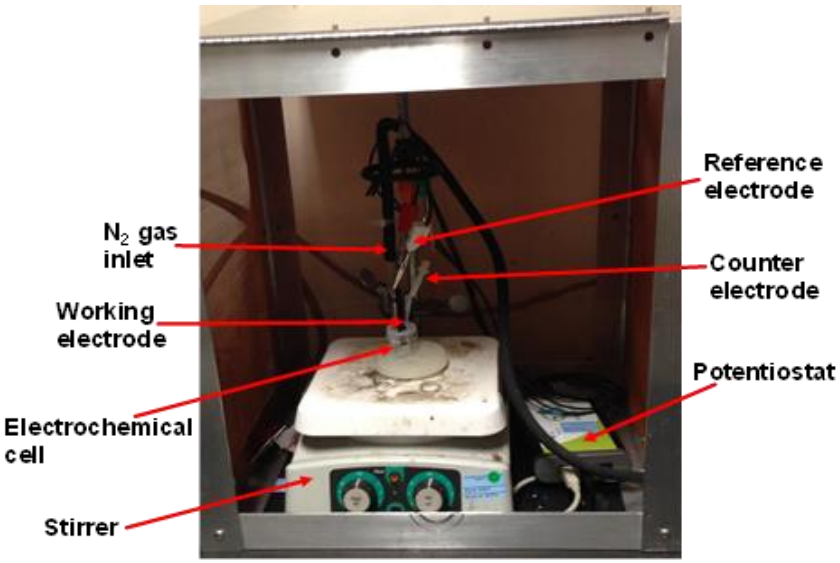

Fig 8. Setup for the electrochemical cell

Spectral analysis and calculation

As the potential is scanning negatively from left to right in blue line, the cathodic peak is increasing due to the reduction of analytes. And the red line shows the oxidation peak current as scanning of potential increasing from beginning. The height of peak belong the concentration of analytes. For perfectly reversible reaction, it generates a duck shaped voltammogram. The peak current is given by the Randles Sevcik equation: $i_p = 2.99x10^5 n^{3/2} ACD^{1/2} v^{1/2}$ and also the peak current can be observed from voltammogram.

n = number of electrons transferred/molecule C = concentration (mol cm^{-3})

A = electrode surface area (cm^2) D = diffusion coefficient (cm^2 s^{-1})

v = sweep rate (Vs^{-1})

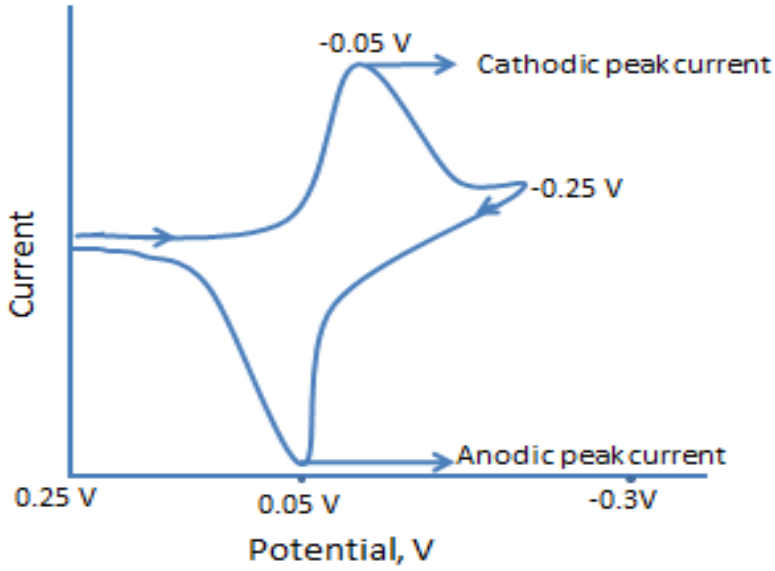

Fig 9. Duck shaped cyclic voltammogram

The sweeping potential in the above voltammogram goes from 0.2 V to -0.25 V, the switching potential. The slight increase in current with increasing potential is due to the capacitance current. At -0.05 V, the peak current appeared due to the reduction of

analytes. The sweeping potentials increased from -0.25 V to 0.2 V. The slight increase in current is again due to the capacitance current originating from electric double-layer formation around the electrode surface. The peak current that appeared at 0.05 V is an anodic current produced due to the oxidation of analytes. The two peaks are separated due to the diffusion of the analyte to and from the electrode.

Potentiostat

A potentiostat is an electronic device that both measures and manages the potential difference between two electrodes. Its key benefit lies in its precise control over applied potential, unlike other normal power sources. By applying potential to an electrode surface, it either decreases or increases the electrons on that surface. Consequently, the surrounding liquid is prompted to either release or absorb electrons to balance this change. A potentiostat can be used in the fields of electrochemistry and biochemistry, but also sensor development and battery research.

Surface characterisation of electrode

Scanning electron microscopy (SEM) and its application

SEM is a powerful tool for imaging the micro to nanostructure of materials. The interaction of the electron beam with the sample surface generates signals that can provide various insights into the material's composition, morphology, and other characteristics. Electrons in a beam are accelerated towards a sample, causing the ejection of core electrons (known as secondary electrons). When incident electrons interact with atoms, some get deflected, leading to the creation of deflected electrons and backscattered deflected electrons. These secondary and backscattered electrons generate highly magnified images, revealing the morphology of the substances being analysed. When a core electron is knocked out, an

electron from a higher shell descends to fill the lower energy level, emitting characteristic X-rays. These X-rays play a crucial role in elemental analysis. The size of nanoparticle deposited on the electrode surface is measured by SEM. The SEM is a relatively non-destructive technique. In our study we observe the carbon dots agglomeration on the electrode surface. By measuring the size of CDs, the histogram of size distribution of is made by using software Image J.

Energy-dispersive X-ray spectroscopy (EDX)

Energy-dispersive X-ray spectroscopy (EDX) is an analytical method used for identifying the chemical composition of materials. When a sample is stimulated by an energy source, like an electron beam in a microscope, it emits characteristic X-rays. These X-rays, generated as electrons transition within the atoms, produce a unique spectrum revealing the elements present. By analysing the peaks' positions, we determine which elements are there, while the signal's strength indicates their concentrations. Ultimately, EDX helps analyse a sample's composition based on the X-rays it emits when excited. SEM in association with EDX provides insight into the particle's shape, size, and elemental composition.

Research objectives

The graphene defects within the carbon dots have been found to alter the electrochemical sensing behaviour of carbon nanomaterial. Changing the precursor materials and methodology, the graphene defects can be controlled. The insight into graphene defects helps to choose the correct electrode materials to construct the biosensor. The detection of dopamine with catecholamine is crucial but challenging. The prevalent technologies to detect the dopamine level in body fluid are expensive. Conversely, the electro analytical methods are less costly and equally applicable for in vivo and in vitro analyses.

Chapter II

Experimental

The research involves the simultaneous detection of dopamine level and study the correlation of graphene defects in carbon dots and with its electrochemical sensitivity. For the detection of dopamine, sucrose carbon dots (SucCDs) were used as electrode materials. Rafinose carbon dots (RafCDs), sucrose carbon dots (SucCDs), and palatinose carbon dots (PalCDs) were each individually weighed one milligram. Subsequently, each type was mixed separately with 1 ml of 200-proof ethanol to create their suspensions. For the comparison of the sensitivity of different saccharides based CDs, they were drop casted on the polished glassy carbon electrode. Slurry of chitosan was used as encapsulating agent for the CDs on the surface of GCE. The cyclic voltammograms were recorded in standard DA solution by using various CDs. The controlled experiment was done to verify the needs of CDs rather than bare glassy carbon electrode surface. Raman spectra of all 4 types of CDs were recorded to quantify the defects density. The surface characterisation of electrode was done by SEM and EDX. The size distribution of CDs on the surface of glassy carbon electrode was analysed by the histogram generated by Image J software. The elemental analysis of surface of working electrode (glassy carbon electrode) was done by EDX.

Chemicals and materials

- Co_3O_4, cobalt oxide (Nanostructured and Amorphous Materials, Inc ; 99% purity, Alamos, New mexico, USA)
- Dopamine hydrochloride (Sigma-Aldrich, St. Louis, MO, USA)
- Phosphate Buffer Solution (PBS), pH 7.00 (Sigma-Aldrich, St. Louis, MO, USA)
- Simulated Urine Normal (Carolina biological supply company)
- Chitosan low molecular weight (Sigma-Aldrich, St. Louis, MO, USA)
- Uric acid (Sigma-Aldrich, St. Louis, MO, USA)
- L-Ascorbic acid (Sigma-Aldrich, St. Louis, MO, USA)
- Sodium bicarbonate (Sigma-Aldrich, St. Louis, MO, USA)
- Homovanillic acid (Sigma-Aldrich, St. Louis, MO, USA)

Preparation of saccharides based CDs

Saccharides CDs were obtained from the Leblanc lab. They were produced by subjecting 20 mL of a 0.3 M saccharide solution (rafinose, sucrose, or palatinose) to hydrothermal treatment. The solution was placed in a Teflon-coated reactor, heated to 200 °C for 30 minutes, and maintained at that temperature for 5 hours. After cooling, solid material was separated through centrifugation, and the supernatant was filtered to remove fine particles. The pH was adjusted to 8 using saturated NaOH solution. The solution underwent dialysis against DI-H_2O for 3 days using a 1 kDa MWCO dialysis membrane, with water changes every 10–12 hours. Finally, the resulting solution was lyophilized to obtain a solid product [44].

Drying of CDs

Sucrose and palatinose are both disaccharides, while raffinose is classified as an oligosaccharide. These sugars exhibit hygroscopic properties. Instead of employing direct heat to eliminate moisture, a vacuum desiccator offers an alternative method. The containers housing of raffinose Carbon Dots (RafCDs), sucrose carbon dots (SucCDs), and palatinose carbon dots (PalCDs) were opened and placed in a vacuum desiccator overnight to extract the moisture linked with the carbon dots. It was observed that carbon dots derived from saccharides melted below 100°C. Which is why CDs were not dried in the oven.

Preparation of CD suspension

One milligram of sucrose carbon dots (SucCDs) was added to a vial containing 200-proof ethanol (absolute anhydrous ethanol). The same process was repeated for raffinose carbon dots (RafCDs) and palatinose carbon dots (PalCDs). The mixture of ethanol and carbon dots underwent sonication for 5 minutes using the Sharpertek Stamina XP^{TM} ultrasonic cleaner (WI, USA). Similarly, a suspension of raffinose carbon dots (RafCDs) and palatinose (PalCDs) carbon dots were prepared. Despite the relatively good solubility of saccharide-based carbon dots in water, their suspension was created in anhydrous ethanol. This choice was made because ethanol readily evaporates from the electrode surface, allowing the carbon dots to adhere to the glassy carbon electrode surface.

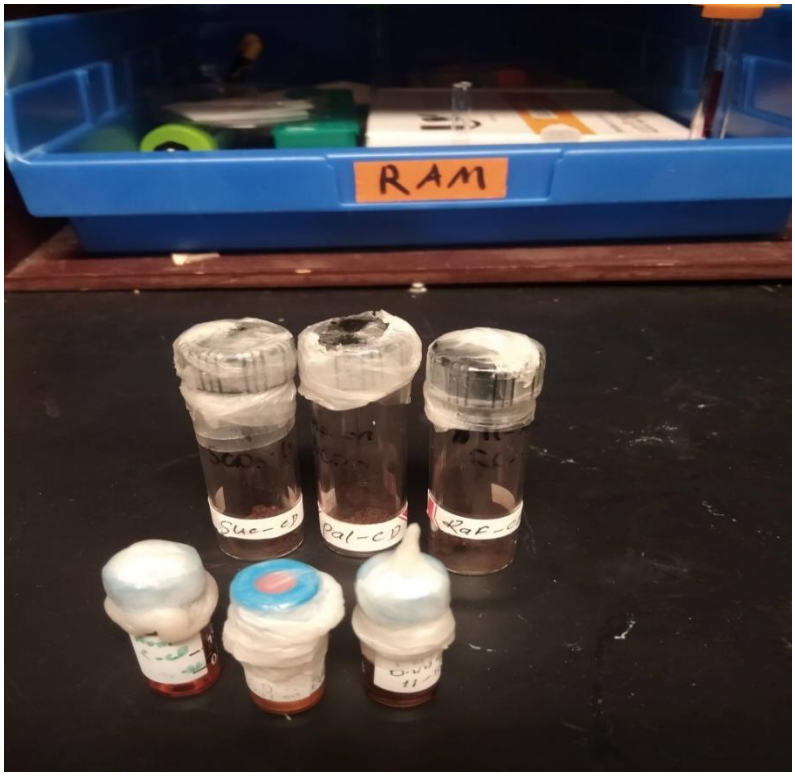

Fig 10. CDs and their suspension in pure and dry ethanol in the concentration of 1mg of CDs per ml of solvent.

Ethanol does not react with saccharides bases carbon dots. Furthermore ethanol is volatile solvent which can be easily evaporated leaving the CDs on the surface of electrode.

Preparation of 5% (w/w) chitosan solution

Chitosan is the biopolymer derived from deacetylation of chitin. It is a linear cationic biopolymer composed of glucosamine and *N*-acetyl-glucosamine. It is soluble in acidic medium and insoluble in neutral and basic medium.

Procedure

2% acetic acid solution was made by adding 1 ml of glacial acetic acid in 19 ml of deionized water. 1.05 g of chitosan is gradually added with continue magnetic stirring for 1 hour. The viscous solution of chitosan has light yellow color. The chitosan is stored in refrigerator at 4^{o} C.

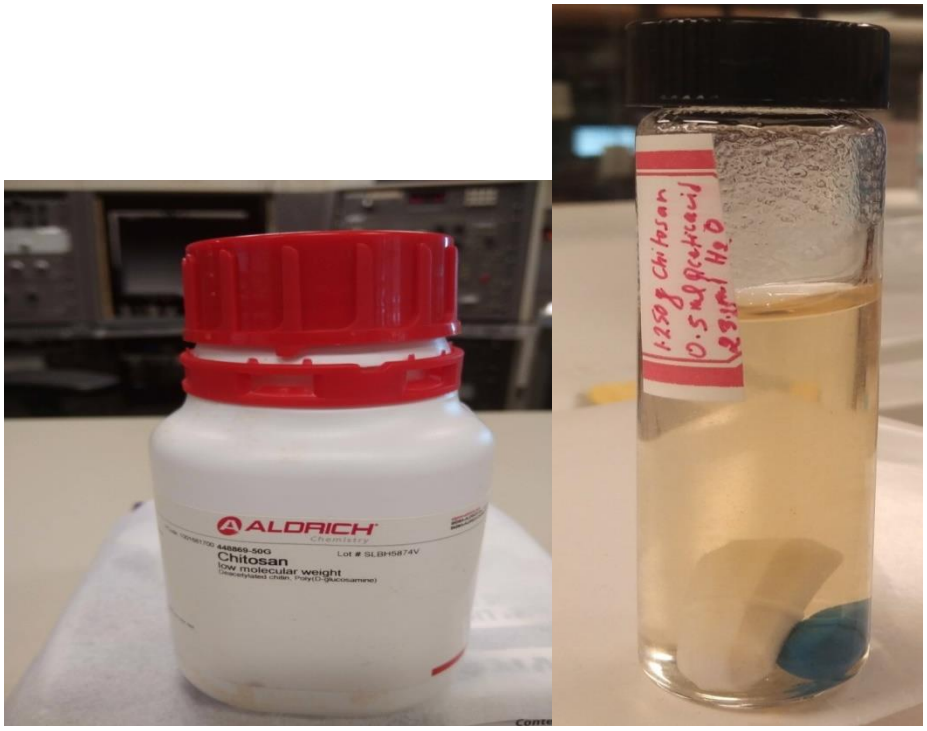

Fig 11. Chitosan and 5% chitosan solution made in 2% acetic acid solution

Activation of electrode

The electrode after sonication is activated by the help of 0.1M $NaHCO_3$ solution. A 20 ml 0.1 M solution is made by mixing 168.9 mg of sodium bicarbonate and 20 ml deionized water. The polished and clean GCE is electrochemically activated by immersing in 0.1 M $NaHCO_3$ solution, and the potential was cycled between -1.149 V and +2.100 V vs Ag/AgCl at a scan rate 100 mV/s for 6 complete cycles.

Calculation of mass of $NaHCO_3$ required preparing 20 ml 0.1 M solution

Mol. Mass of $NaHCO_3$ = 84.01 g/mole

% purity by weight = 99.5%

Volume of solution required =20 ml

Molarity = No. of mole /Volume of solution in litres

Molarity = $$\frac{Mass\ required\ (g)}{Molar\ mass\left(\frac{g}{mol}\right)\times Volume\ of\ solution\ (L)}$$

Mass required = $V(l)\ \times\ M\ (\frac{mol}{L}) \times Mol\ mass\ (\frac{g}{mol})$

$= 0.02l\ \times 0.1\ \frac{Mol}{L} \times 84.01\frac{g}{mole}$

= 168.01 g of 99.5% pure

Glassy Carbon electrode (GCE) surface modification by CDs

The carbon dots (CDs) is applied to the glassy carbon electrode surface using the drop-casting method, as described by Wayu et al [43]. Initially, the glassy carbon electrode was polished on a Nylon Polishing Cloth using 1.0 µm sized alumina slurry for 3 minutes, employing circular motions. Subsequently, the polished electrode surface was rinsed with deionized water and immersed in a plastic tube filled with deionized water, then subjected to 5 minutes of sonication. After sonication, the electrode surface was rinsed again and polished for 3 minutes using 0.05 µm alumina slurry. Throughout the successive polishing stages, the polish pad was regularly cleaned using chem wipes. After the final polishing, the electrode was rinsed with deionized water, underwent a 5-minute sonication in deionized water, and further sonicated in a 1:1 water-HCl solution for five minutes. Then electrode was activated. To activates the electrode, a 0.1 M sodium bicarbonate solution was prepared in distilled water. The freshly polished electrode underwent 10 consecutive cycles of cyclic voltammetry (CV). The upper potential was fixed at 2.100 V, while the lower potential was set to -1.145 V during the recording process.

Cyclic voltammogram was recorded with the following parameter

Scan rate =50 mV/S potential scan range -1 V to 0.8 V relaxation time 3 second

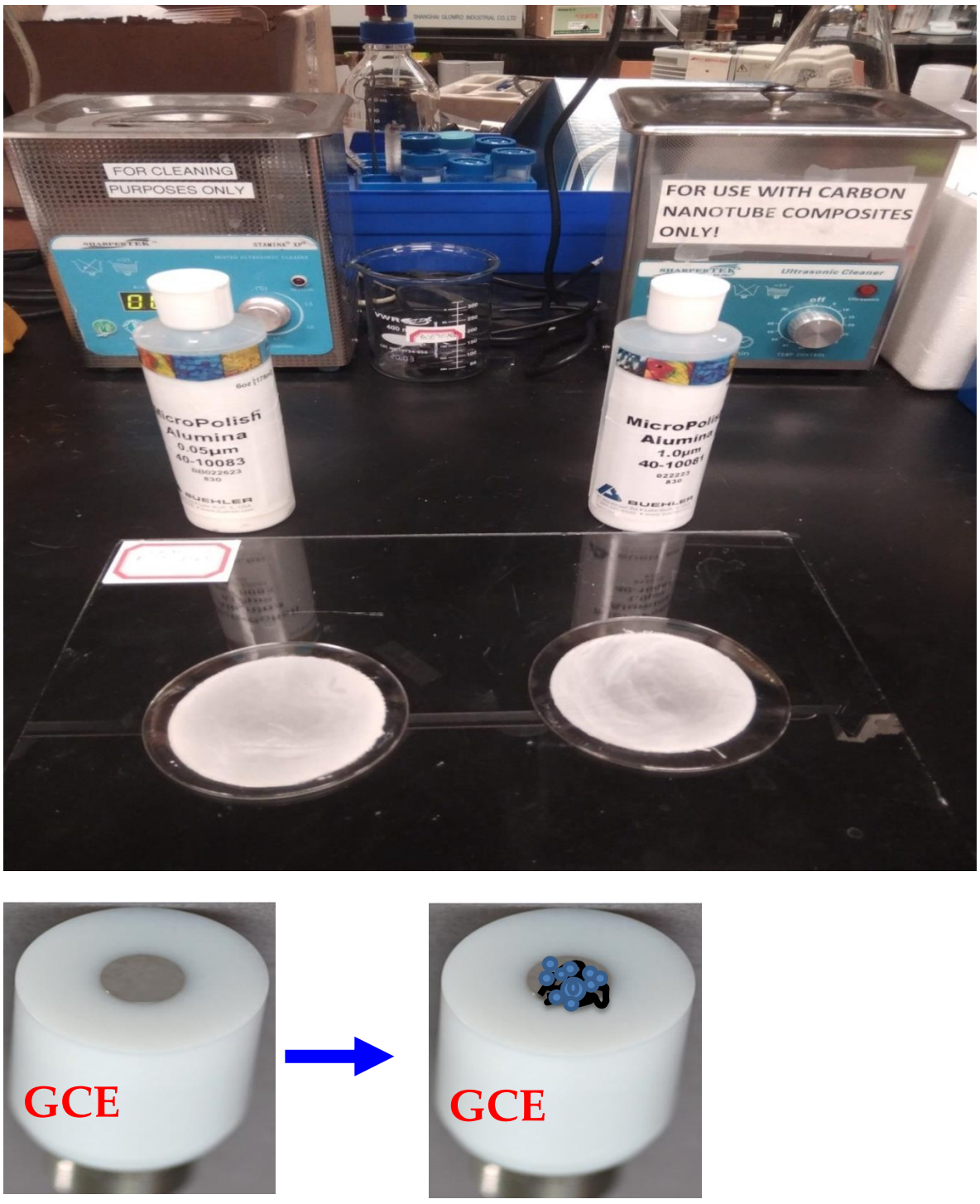

Fig. 12. Work station (above) and polished glassy carbon electrode and glassy carbon electrode with CDs.

Electrochemical detection of Dopamine

Cyclic voltammetry (CV) technique was employed to study the detection of DA concentration. Manually constructed faraday case could be used to block the electromagnetic radiation. I have not encountered such interference of electromagnetic radiation; therefore, I did my experiment outside the Faraday case. The cyclic voltammetry experiment was carried out in the Pine Research electrochemical cell made up of glass. The potential range was set at -1.0 to +0.80 V at the scanning rate of 50 mV/s. Voltammetry using Wave Nano potentiostat. Aftermath electrochemical software (Version 1.4.7881 by Pine instruments, Raleigh, NC, USA) is used to record and display the result of cyclic voltammetry. The potentiostat connects to the three electrodes of electrochemical cell. These three electrodes are working electrode, modified glassy carbon electrode (GCE/reference electrode, and counter electrode. The working electrode is modified glassy carbon electrode (GSE/SucCDs/Chitosan), reference electrode, Ag/AgCl (4 M KCl) and counter electrode platinum wire. Phosphate buffer solution (PBS) of pH 7 is used as a solvent to dissolve the dopamine.

Defect quantification by Raman spectroscopy

Horiba Raman spectrometer was employed to quantify the defect density in carbon dots. Each type of carbon dot—SucCDs, RafCDs, PalCDs, and FruCDs—were placed directly onto separate microscopic glass slides for the Raman experiments, requiring no additional sample preparation. These slides, each containing the respective carbon dots, were inserted into the instrument's case after calibrating it for both 534 nm and 785 nm lasers.

Initially, the sample was focused and its position secured. A 50x magnification lens was chosen to precisely focus the laser onto the sample surface. For the Raman experiment, the settings were adjusted to utilize a 534 nm laser at 5% power, with an acquisition time of 10 seconds and 12 accumulations. Subsequently, spectra were recorded for all the mentioned types of carbon dots. The Raman data was extracted in excels format and plot in the Origin Pro 8.5.

CHAPTER III

RESULTS AND DISCUSSION

Raman spectroscopy is used to quantify the defects density by calculation of D/G band ratio. The size of carbon dots and their agglomeration was studied by scanning electron microscopy (SEM) and the elemental analysis of electrode surface was done by the energy dispersive spectroscopy (EDS). The electrocatalytic behaviour of composite electrode was studied with cyclic voltammetry.

Raman Spectroscopy Analysis of RafCDs, PalCDs, and SucCDs

The disorder level within the graphene sheet correlates with the presence of sp^3 hybridized carbon in these carbon dots (CDs). Pristine graphene typically comprises hexagonally arranged sp^2 hybridized carbon. In the Raman spectra, distinctive peaks, namely the D band at 1333 cm^{-1} and the G band at 1588 cm^{-1}, are observed. The respective peak areas are indicative of their concentrations. Although the spectra originate from a microscopic portion of the sample, their implications can be extended to the entire bulk.

The ratio of the D band to the G band differs among the CDs: SucCDs (0.195), PalCDs (0.117), and RafCDs (0.097). SucCDs exhibit the highest defect density, correlating with maximum electrochemical sensitivity. Specifically, the anodic peak current, measured in a 0.1 mM dopamine solution in PBS at pH 7, shows a trend: SucCDs (51 µA) exhibit the highest current, followed by PalCDs (46.12 µA) and RafCDs (36 µA) successively. The magnitude of anodic currents increases with higher defect density. Defects enhance electron density by establishing electron sinks within the lattice, thereby facilitating

electron transfer acceleration. The electrochemical sensing property is notably enhanced within the potential range of -0.2 V to +0.3 V due to the defects and beside that potential range, it is not found to be true. Prussian Blue-ZnO/COOH-MWNTs, for H_2O_2 detection at +0.0004 V, defects increased sensitivity by 2.7-fold [45]. SucCDs have highest defects density followed by PalCDs and RafCDs which are correlated with the electrochemical sensing of DA in PBS pH 7. The result is in the agreement of the assumption made by density functional theory calculations (applying Gerischer model) predict that for aqueous solution reactions near the Fermi level (-0.2 to +0.3 V) standard potential vs SHE, an increase in defects (sp^3 carbon) enhances electron transfer [46].

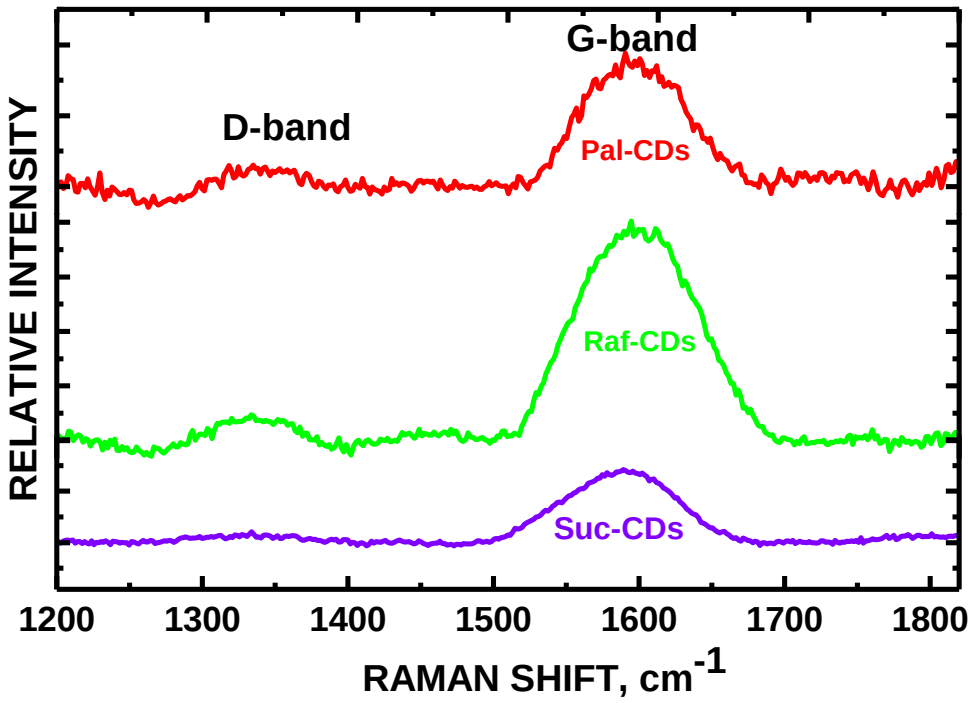

Fig 13. Stack plot of SucCDs, RafCDs, and PalCDs

Raffinose carbon dots exhibit the highest exposed graphene, while sucrose has the lowest, followed by palatinose. Sucrose is identified as the most effective for the electrochemical sensing of dopamine, followed by palatinose and raffinose. The sensing property is

enhanced with higher defect density, especially when the redox potential aligns closely with the Fermi level, consistent with findings in the literature [46].

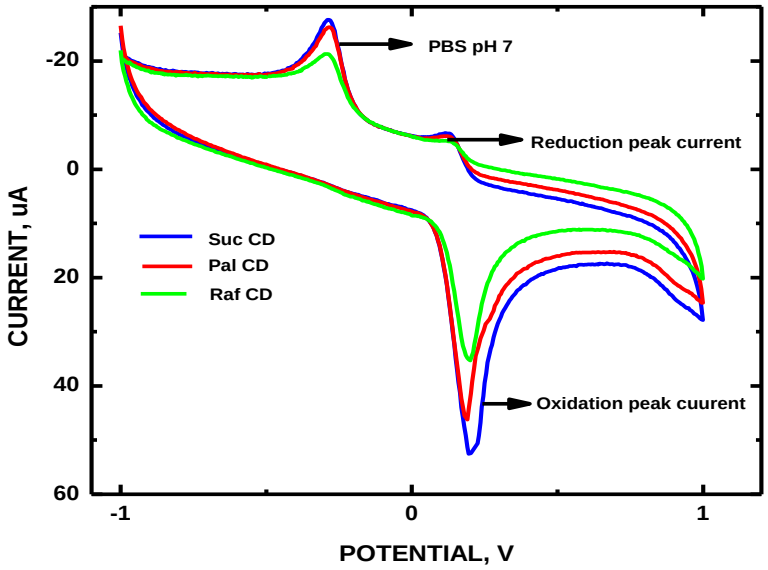

Fig 14. CVs of SucCDs, PalCDs, and RafCDs in 0.3 mM DA in PBS pH 7

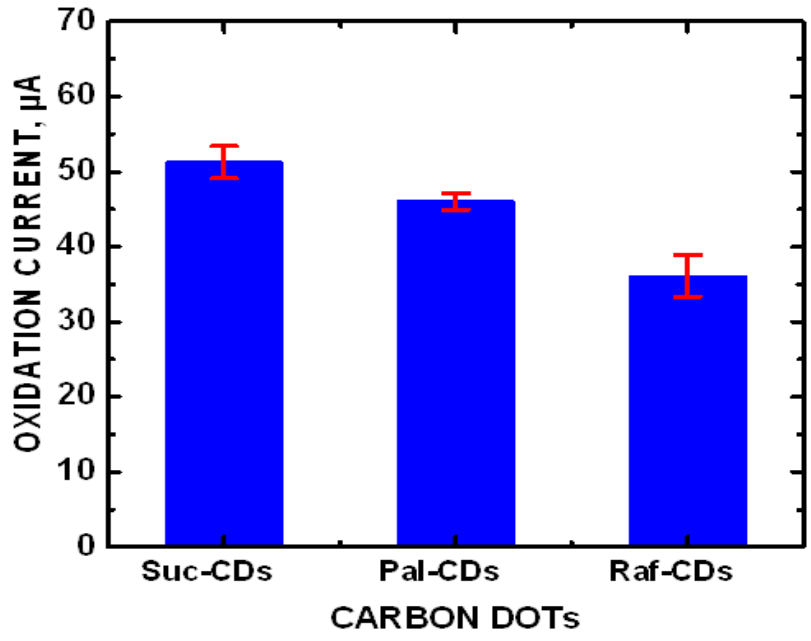

Fig 15. SucCDs, PalCDs, and RafCDs for their utility of electrochemical sensing of Dopamine

The anodic peak current was measured in 100 µM DA solutions in phosphate buffer solution of pH 7.

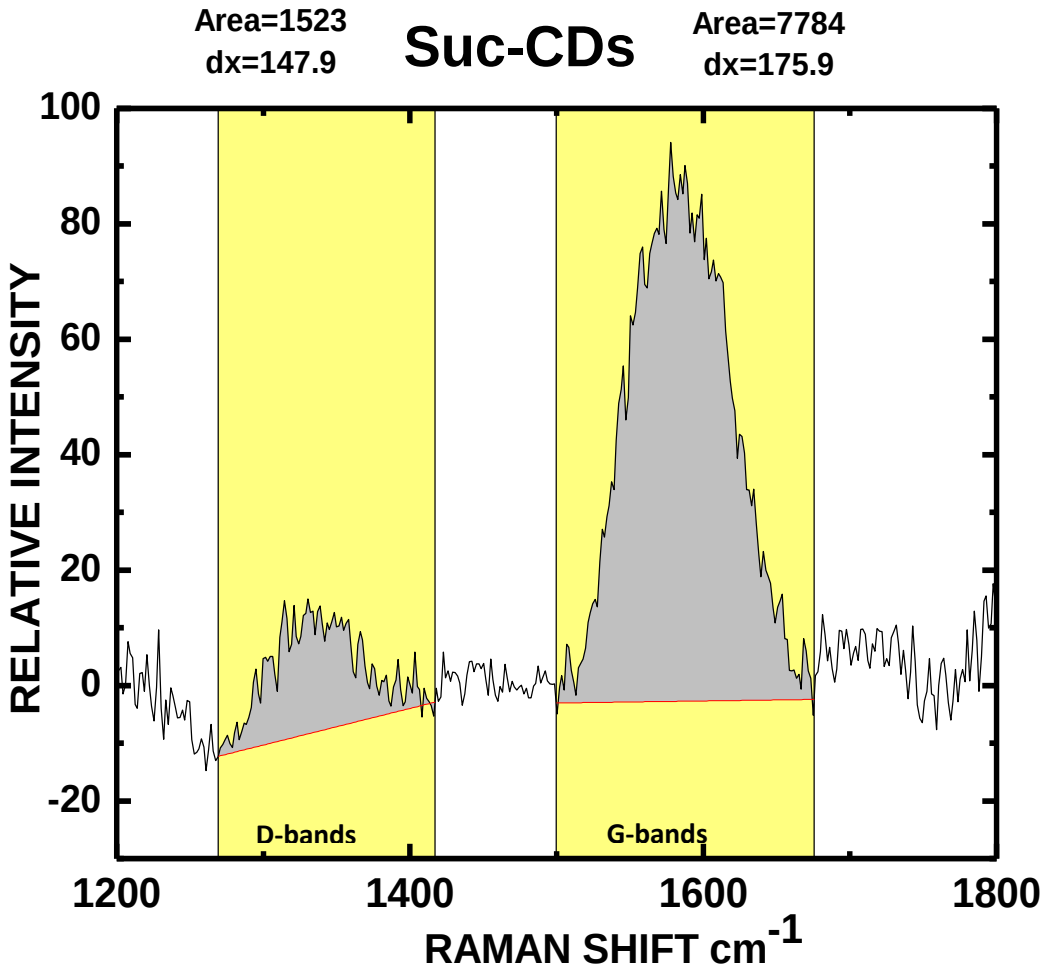

Fig 16. Raman spectra of Suc-CDs showing the intensity of a D-band and a G-band

The peak areas of the D-band represent the defects concentration in the graphene sheet and where each carbon is in sp^3 hybridization. On the other hand, the peak area of the G-band represents the concentration of exposed graphene sheet where carbon is in sp^2 hybridization.

Peak area of D-band = 1523

Peak area of G-band = 7784

The defects density is calculated as I_D/I_G = 1523/77 = 0.195

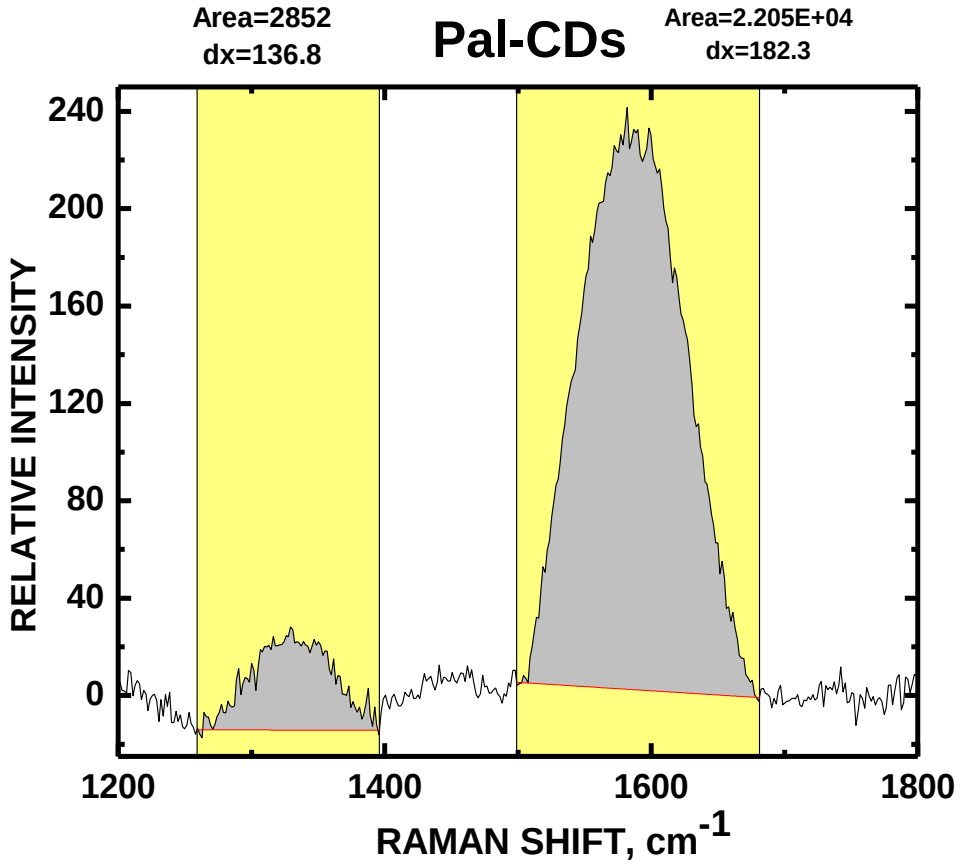

Fig 17. Raman spectra of Pal-CDs showing the intensity of a D-band and a G-band

The peak areas of the D-band represent the defects concentration in the graphene sheet and where each carbon is in sp^3 hybridization. On the other hand, the peak area of the G-band represents the concentration of exposed graphene sheet where carbon is in sp^2 hybridization.

Peak area of D-band = 2852

Peak area of G-band = 22050

The defects density is calculated as I_D/I_G = 0.115

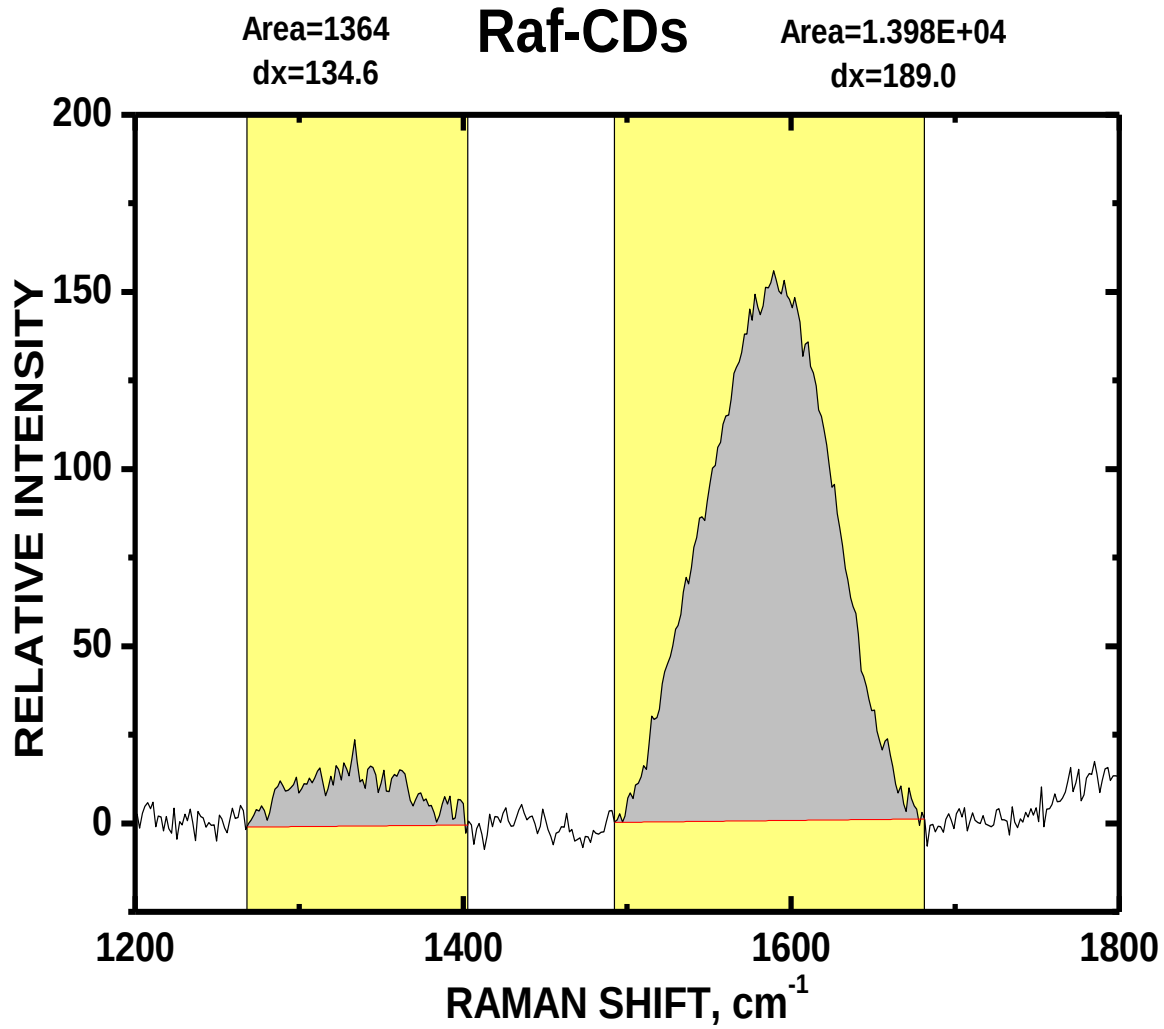

Fig 18. Raman spectra of RafCDs showing the intensity of a D-band and a G-band

The peak areas of the D-band represent the defects concentration in the graphene sheet and where each carbon is in sp^3 hybridization. On the other hand, the peak area of the G-band represents the concentration of exposed graphene sheet where carbon is in sp^2 hybridization.

Peak area of D-bands = 1364 Peak area of G-bands = 13980

The defects density is calculated as I_D/I_G =0.0975

The SucCDs has highest defect density which is correlated with its greatest electrochemical sensing of dopamine. The result is in agreement with following previous results.

Prussian Blue-ZnO/COOH-MWNTs, for H_2O_2 detection at +0.0004 V, defects increased sensitivity by 2.7-fold [45]. CoO/COOH-MWNTs, for DA detection at +0.3 V, defects increased the sensitivity for the analyte [47]. The sensitivity of GalCDs, LacCDs, and GluCDs for detecting acetaminophen at +0.549 V decreased with an increase in sp3 carbon density [48].

In this research, the defect density decreases in the order of Suc CDs > PalCDs > RafCDs while the electro catalytic sensitivity measured by RafCDs < Pal CDs < SucCDs.

The correlation of defect density with electrochemical sensing of DA is best described

CDs	Defect density I_D/I_G	Anodic peak current, μA
SucCD	0.195	52.53
PalCD	0.115	46.37
RafCD	0.0975	35.35

Table 1. Correlation between defects density and their electrochemical sensitivity

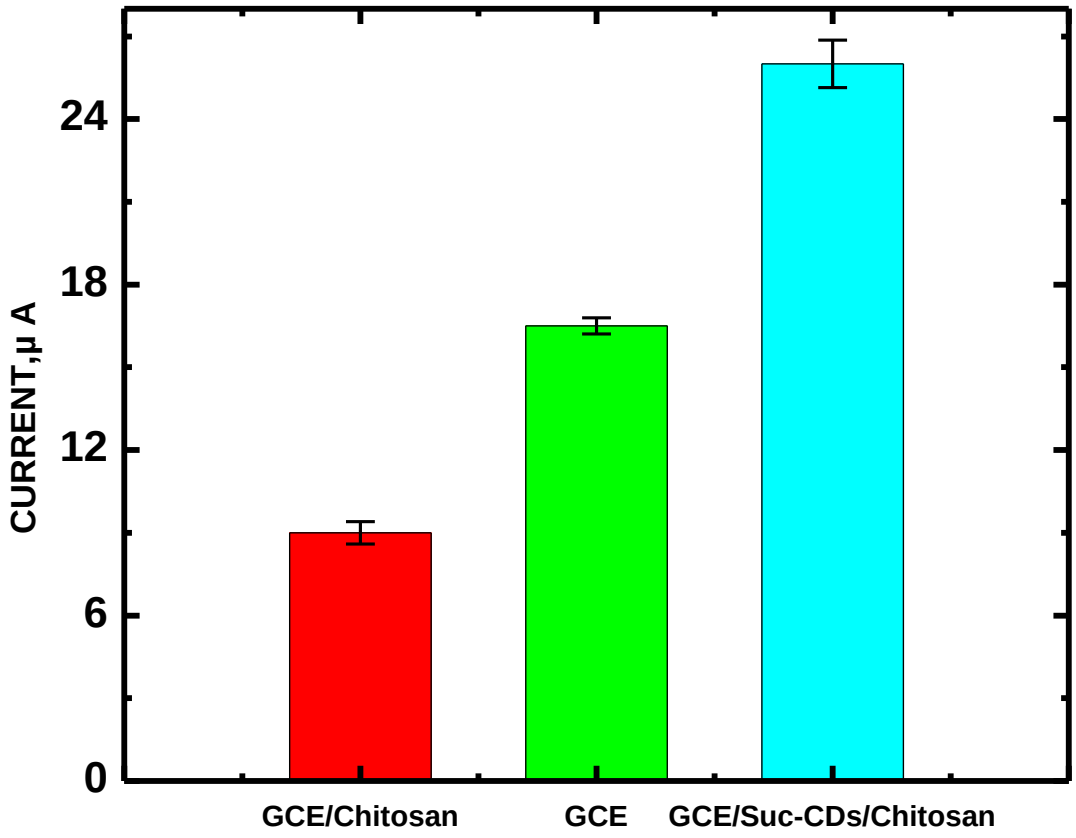

Fig 19. Control conductivity experiments of conductivity

The bar chart shows the carbon dot is better catalyst for electrochemical sensing of dopamine. Chitosan, a biopolymer derived from the de-acetylation of chitin, exhibits lower conductivity compared to the surface of a glassy carbon electrode (GCE). However, incorporating SucCDs onto the GCE surface, encapsulated by chitosan, enhances the electrode's conductivity.

Scanning Electron Microscopy (SEM)

Suc-CDs are found best for electrosensing of DA. To insight into the morphology of the composite, we record the SEM image of the electrode surface. 10 µL of suspension of Suc-CDs was drop cast on the polished GCE and allowed to air dry. The image of the electrode surface was taken in the absence of chitosan on CDs. The SEM image showed the aggregation of CDs on the surface of GCE. The cause of aggregation might be Van der Waals force of attraction and oxidation of CDs 3 weeks after preparation of electrode.

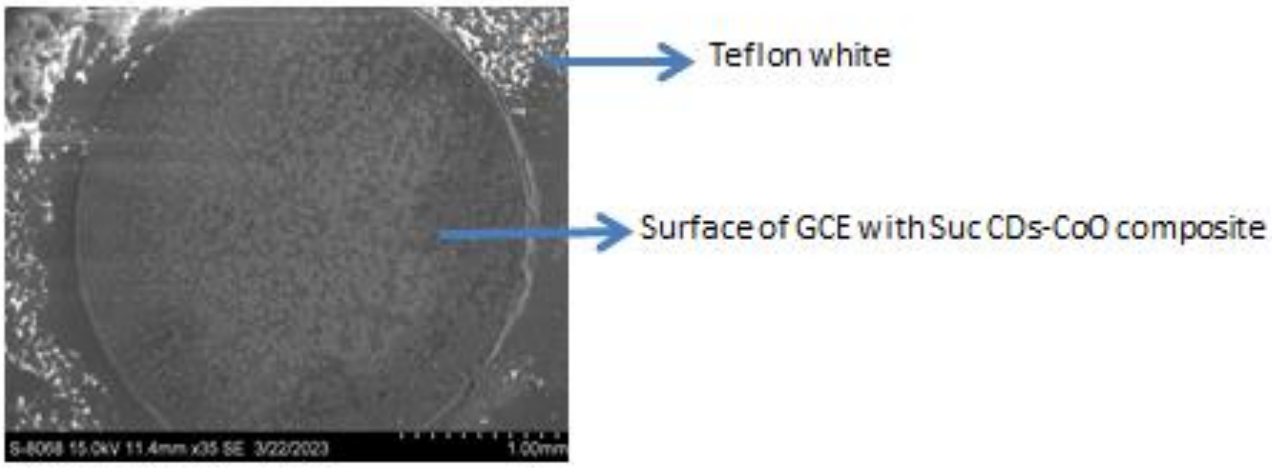

Fig 20. Glassy carbon electrode surface after drop casting of 10 µL of SucCD suspension. Figure shows the excessive aggregation of CDs on the surface of glassy carbon electrode. Vandarwaals force of attraction might be the key factor for the agglomeration of tiny particle to the bigger one.

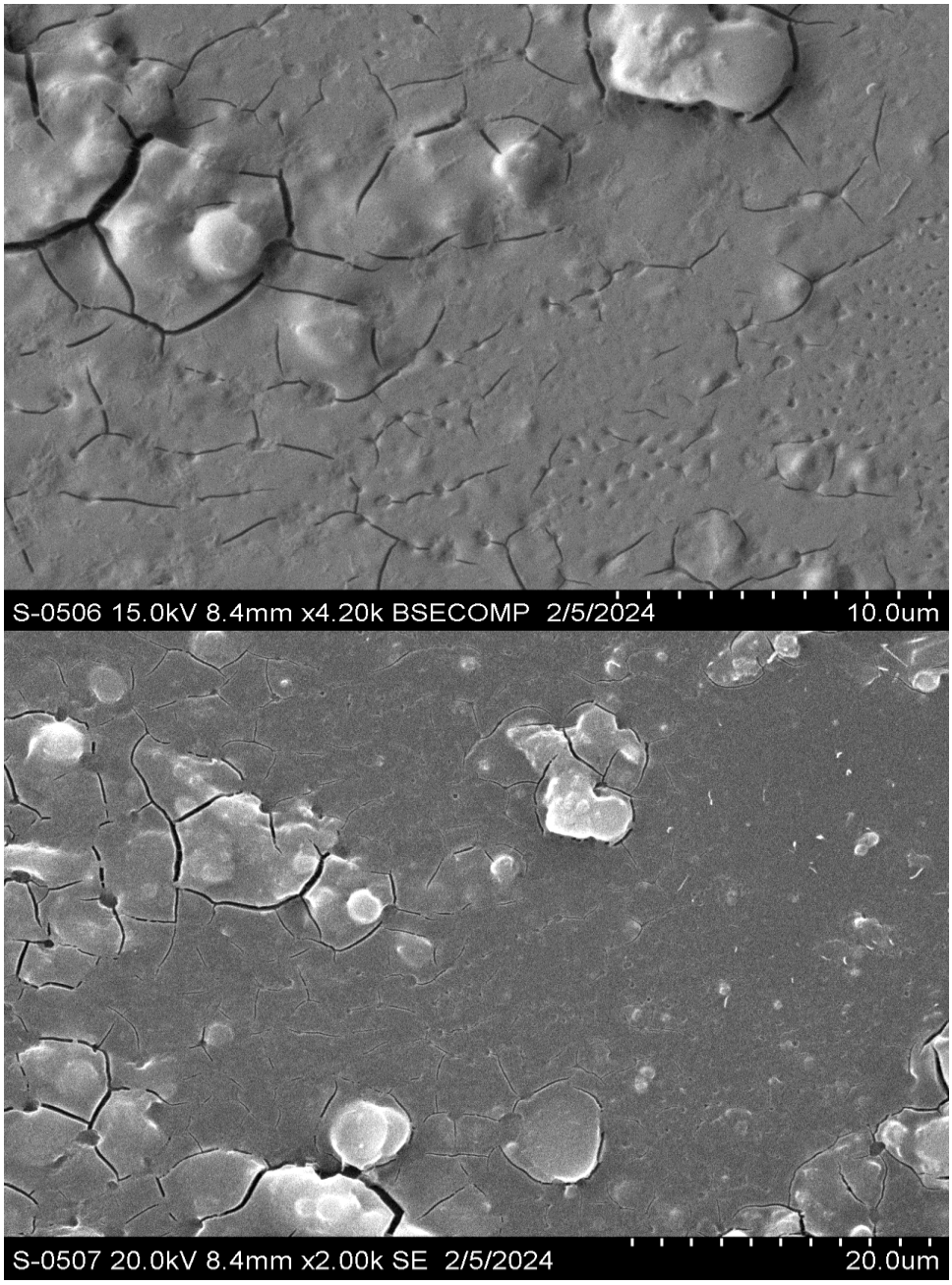

Fig 21. SEM image of SucCDs on the GCE surface after 3 weeks

The above image shows that the carbon dots are no more in nanoparticles size. The image was recorded after 3 weeks of deposition of suspension on the surface of glassy carbon electrode. The CDs are decomposed. CDs are susceptible to oxidation after it is drop casted on the surface of glassy carbon electrode. Saccharides based CDs are stored in vacuum desiccator to prevent it from being oxidized.

Dopamine cyclic voltammetry experiment

The cyclic peak current was measured at nearly 0.2 V. The peak in the -0.3 V is due to the reduction of PBS. Increasing the potential on the working electrode leads to a slight rise in capacitance current due to the formation of an electric double layer. However, a significant current spike occurs around 0.2 V due to dopamine oxidation. As the potential decreases, the oxidized dopamine product is reduced at a similar potential. The slight variation in oxidation and reduction potentials is attributed to analyte diffusion. The cyclic voltammogram confirms that oxidation is more favourable than reduction, with significantly higher peak currents observed during oxidation compared to reduction.

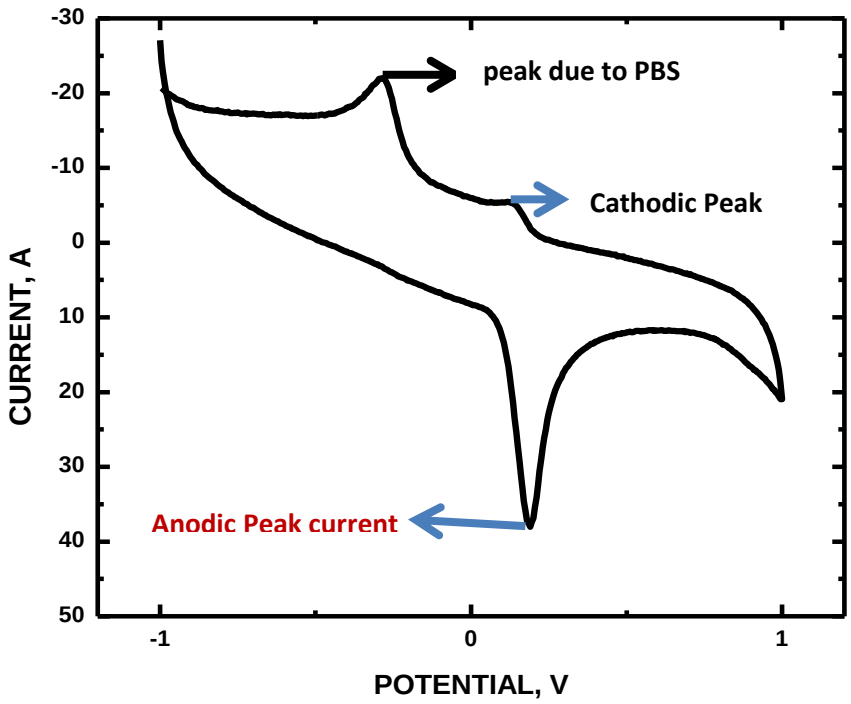

Fig 22. Cyclic Voltammogram of SucCDs in 100 µM dopamine solution in 0.1 mM Phosphate Buffer Solution pH 7.

The difference in between the anodic peak potential and cathodic peak potential is due to the diffusion of dopamine and dopamine-o-quinone to and from the electrode. The oxidation of dopamine is favoured, leading to the formation of the thermodynamically stable product, dopamine ortho-quinone. Consequently, the reversible reaction proceeds slowly, resulting in a small cathodic peak.

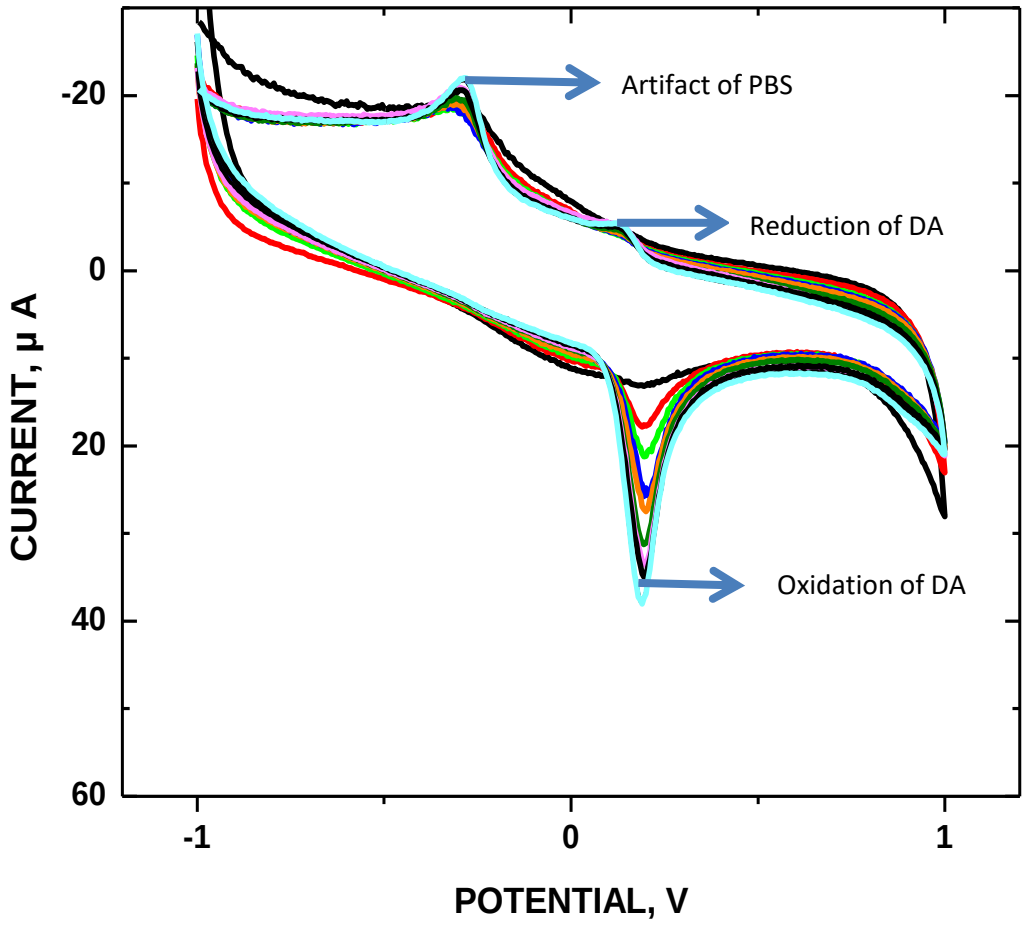

Fig 23. Cyclic voltammetry experiments at different dopamine concentration using Chitoasn/SucCDs/GCE sensor

The concentration of dopamine solution is from 5 to 100 µM which is significance range of concentration of dopamine in the urine of neuroblastoma patents. On increasing the concentration of DA, the anodic peak current as well as cathodic peak current increases. The difference in anodic and cathodic peak potential is due to the diffusion of oxidised and reduced product to and from the electrode.

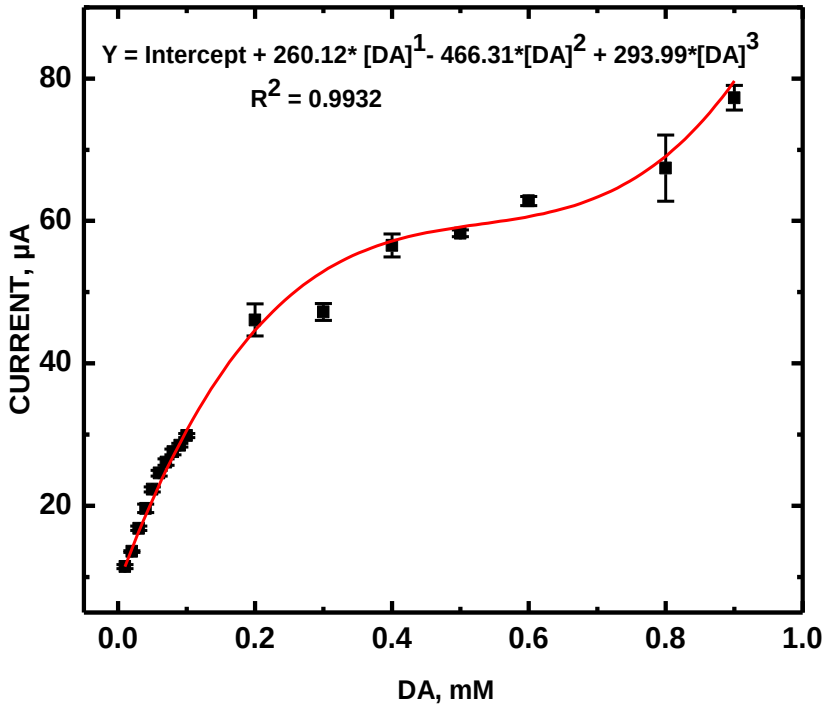

Fig 24. Calibration curve of SucCDs in dopamine (3^{o} polynomial)

Analytically the data points in calibration curve fits cubic polynomial. A calibration curve is made by the measurement of peak current at different concentration of DA. The increase of anodic peak current on increasing the concentration of DA is due to the oxidation of greater number of DA molecule. The lowest concentration measured by the electrode was 5 µM. The solution of dopamine is prepared in the phosphate buffer solution of pH 7.

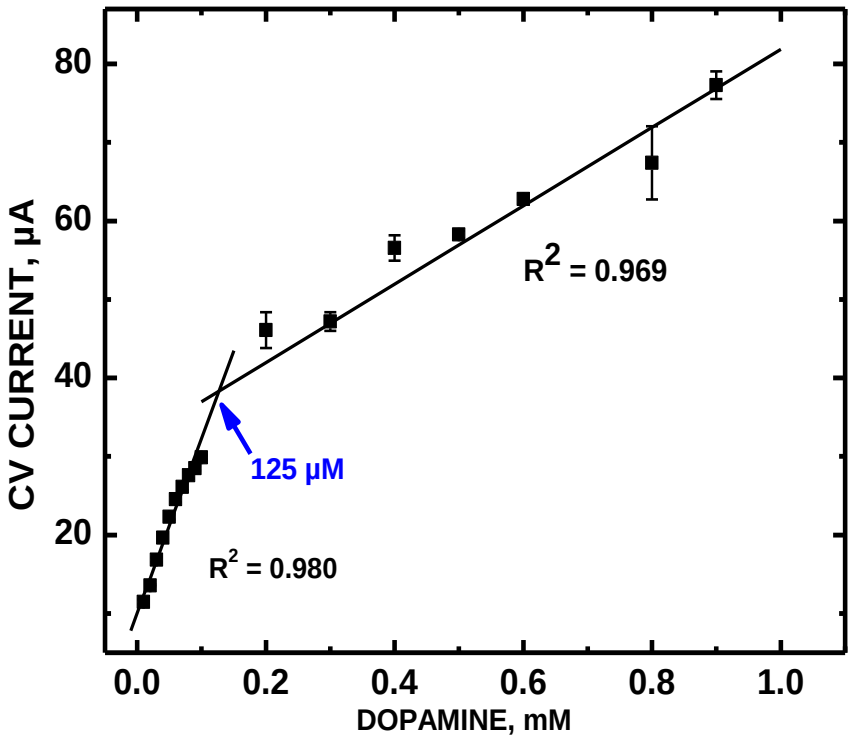

Fig 25. Calibration curve of SucCDs in dopamine

The calibration plot shows that in the lower concentration of DA the slope of concentration vs current is greater than that in higher concentration. In low concentration, the diffusion of analytes is faster consequently the rate of redox phenomenon is higher. At certain concentration, the oxidised product of analytes starts to surround the electrode surface and hinders the diffusion of un-oxidised product towards the electrode. Our results show there is saturation of oxidised products of analytes in the electrode surface at 125 µM. At the break point the dopamine o-quinone surrounds the electrode surface by which hinders the diffusion of dopamine towards the electrode. The electrode surface became saturated with oxidised DA.

Diffusion control experiment

In a diffusion-controlled experiment, a 100 µM dopamine (DA) solution was prepared in a phosphate buffer solution with a pH of 7, employing a scan rate ranging from 10 to 120 mV/s. The anodic peak current exhibited a linear increase relative to the square root of the scan rate. At a temperature of 25°C, the relationship is described by the R-S equation.

$$\mathbf{I_p = 2.69 \times 10^5\, A \cdot (D_{Ox})^{1/2} \cdot n\, (\alpha \cdot n_\alpha)^{1/2}\, .C_{Ox} .\, v^{1/2}} \quad [49]$$

where

I_p = anodic peak current

A = effective surface area of electrode = 0.19625 cm^2

D = coefficient of diffusion = 5.21 x 10^{-5} $cm^2 \cdot s^{-1}$

n_α = number of mole of electron transfer = 2

α = transfer coefficient =1

C = molar concentration = 1.00 x 10^{-7} $mol.cm^{-3}$

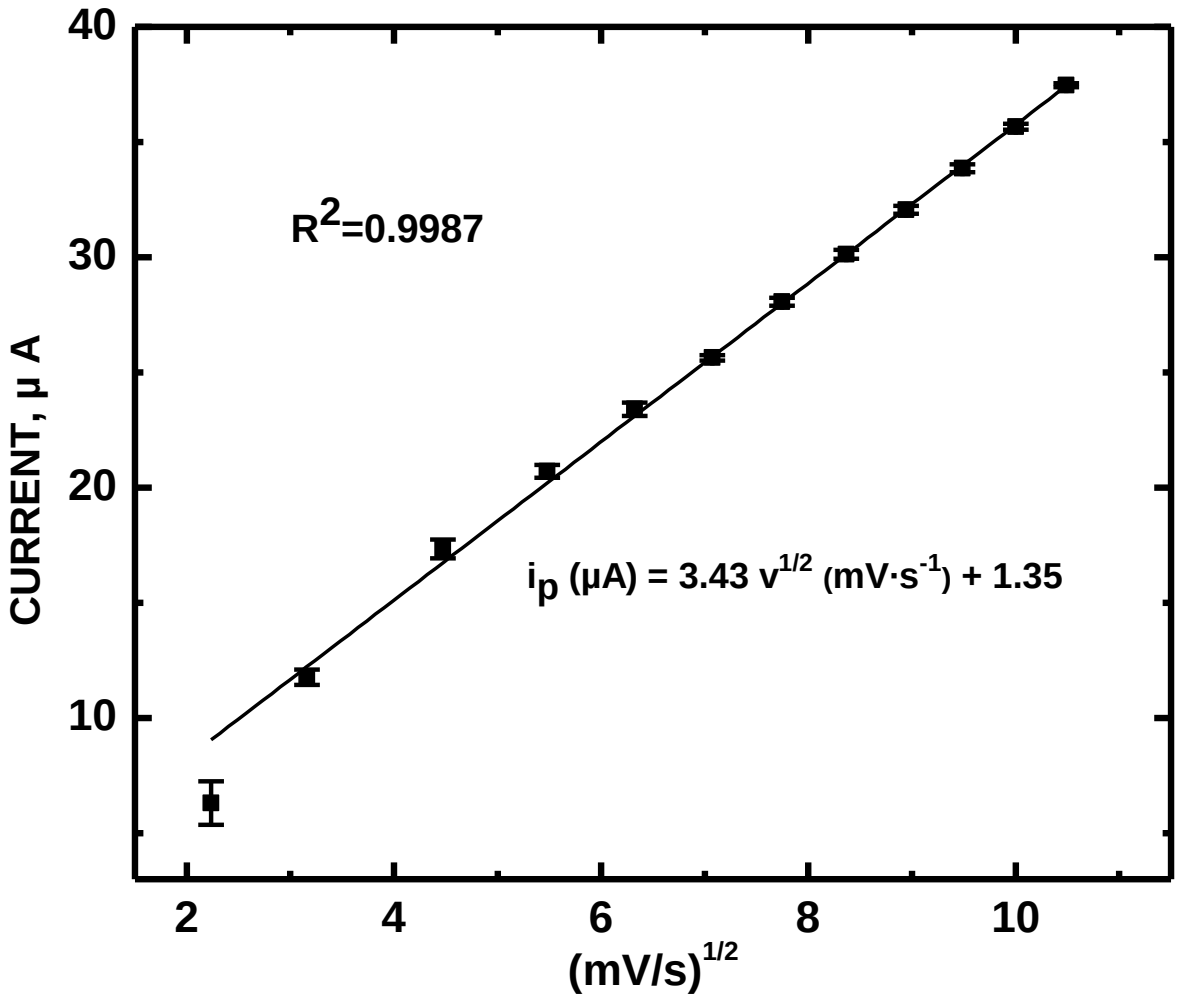

Fig 26. R-S plot SucCDs DA 0.1mM (10mV/S -120 mV/sec)

The diffusion control experiments demonstrate that dopamine exhibits an outstanding diffusion coefficient within sucrose carbon dots, surpassing that in silica nanowires. Specifically, the diffusion coefficient values for dopamine in sucrose carbon dots are significantly higher at 5.21×10^{-5} $cm^2 \cdot s^{-1}$, while in silicon nanowires, the respective values are 2.77×10^{-5} and 2.01×10^{-5} $cm^2 \cdot s^{-1}$. Significantly, the diffusion control value of sucrose carbon dots is double that observed in silicon nanowires [50]

Selectivity study of SucCDs/GCE sensor towards Dopamine

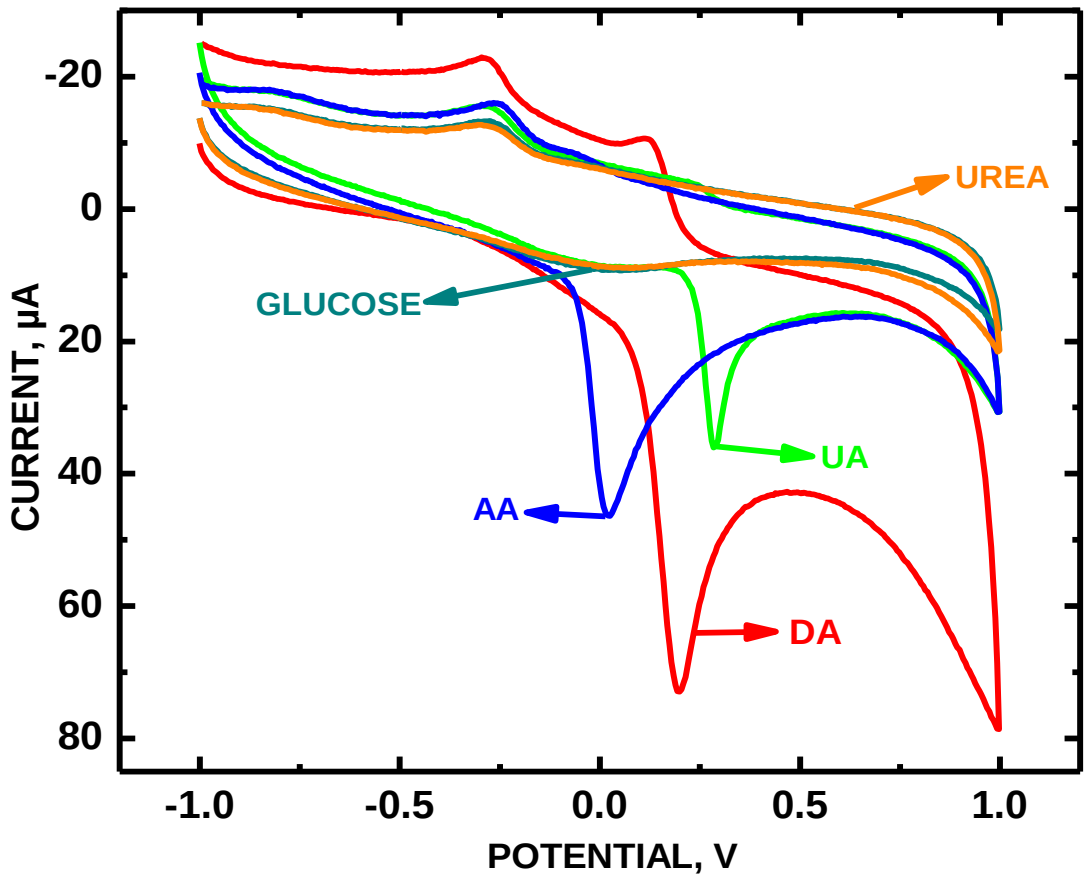

Fig 27. Selectivity test of electrode

In body fluids like urine, dopamine is associated with urea, uric acid, ascorbic acid, and glucose. The chitosan/SucCDs/GCE electrode is selective to the DA. The electrode also response to the ascorbic acid and uric acid in PBS pH 7 but the redox reaction occurs at different potentials.

Rationale to use Co_3O_4-SucCDs instead of using SucCDs

The literature demonstrates that incorporating carboxylic acid functionalized carbon nanotubes into cobalt oxide nanoparticles enhances the signal for dopamine detection. This research was conducted within the same laboratory. In this study, I replaced carbon

nanotubes with carbon dots in the cobalt oxide nanoparticle matrix for dopamine detection in simulated urine.

Concentration of dopamine in urine

The urinary reference ranges for dopamine in children are as follows:

- 0-1 year: 0-85 µg/24 hr
- 1-2 years: 10-140 µg/24 hr
- 2-4 years: 40-260 µg/24 hr
- >4 years: 65-400 µg/24 hr [51]

Considering with a 24-hour urination volume of 200 ml, the regular level of dopamine is 400 µg in the total urine. Molarity of dopamine in normal urine

$= 4.00\times10^{-4}\ \text{g}\ \frac{1}{189.64\ g/mol} \times \frac{1}{0.2l} = 10.56\ \mu\text{M}$

Children with neuroblastoma may exhibit urine dopamine levels that are 10 times higher than normal. Our electrode can precisely detect the 5 µM to 110 µM.

Preparation of sucrose carbon dots cobalt oxide nanoparticles composite

0.7165 mg of SucCD and an equivalent amount of Co_3O_4 ($CoO.Co_2O_3$) were carefully weighed using an ultrasensitive balance and combined in a vial. The suspension of the mixture was created by dissolving it in 1.423 ml of 200-proof ethanol. The resulting mixture was then subjected to sonication using a SHARPER TEX XP-PRO ultrasonicator for duration of 30 minutes.

CV Parameters

The cyclic voltammogram was recorded in the various concentrations of dopamine in simulated urine. The parameters were set as follows

Initial potential = -1 V vs REF Vertex potential = 0.8 V vs REF

Final potential = -1 V vs REF

Sweep rate = 50 mV / s initial electrode range = Highest

Induction period = 3 s Relaxation period = 1

Cyclic voltammetry experiments at different dopamine concentration using Chitosan/SucCDs/GCE sensor

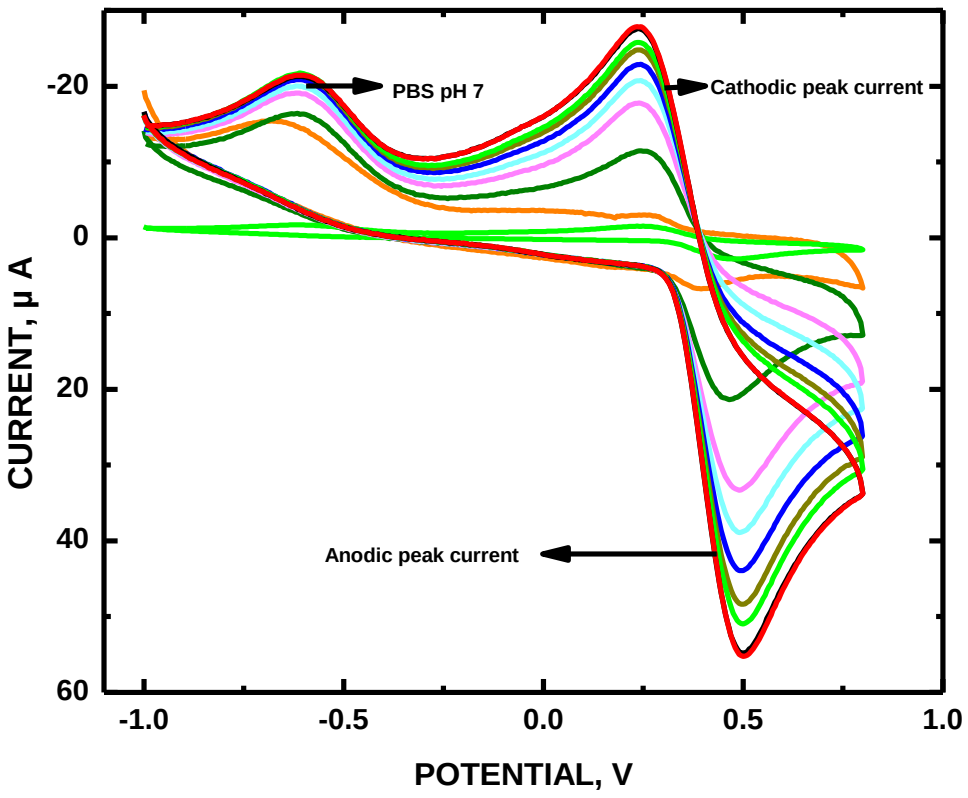

Fig 28. Cyclic voltammogram of Co_3O_4-SucCD with DA (10-100 µM) in simulated urine

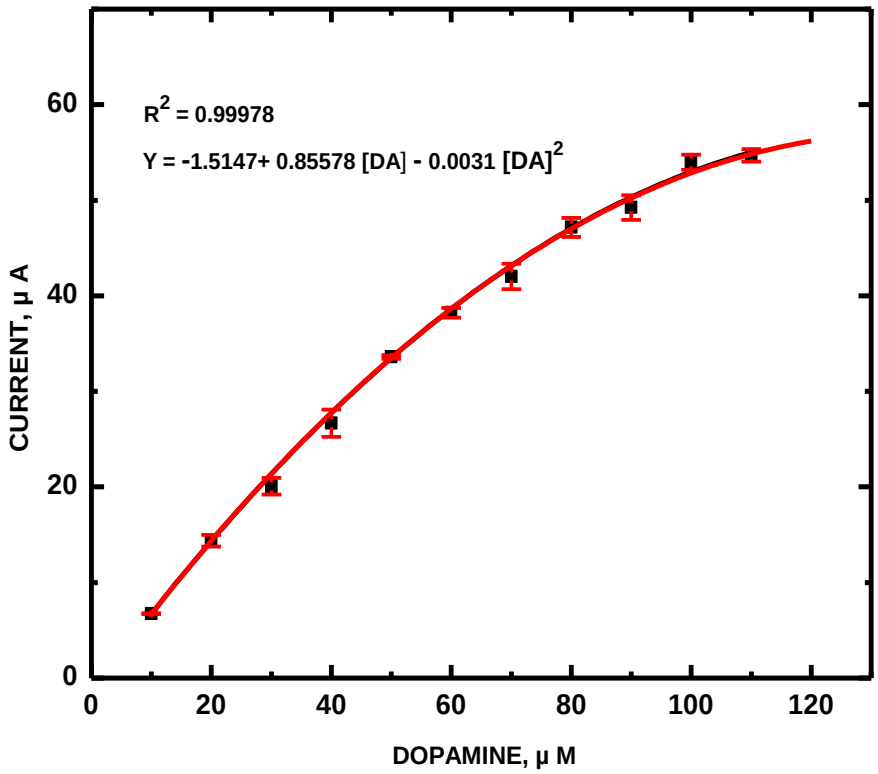

Fig 29. Calibration of Co3O4-SucCDs composite in DA (10-110 µM) in simulated urine

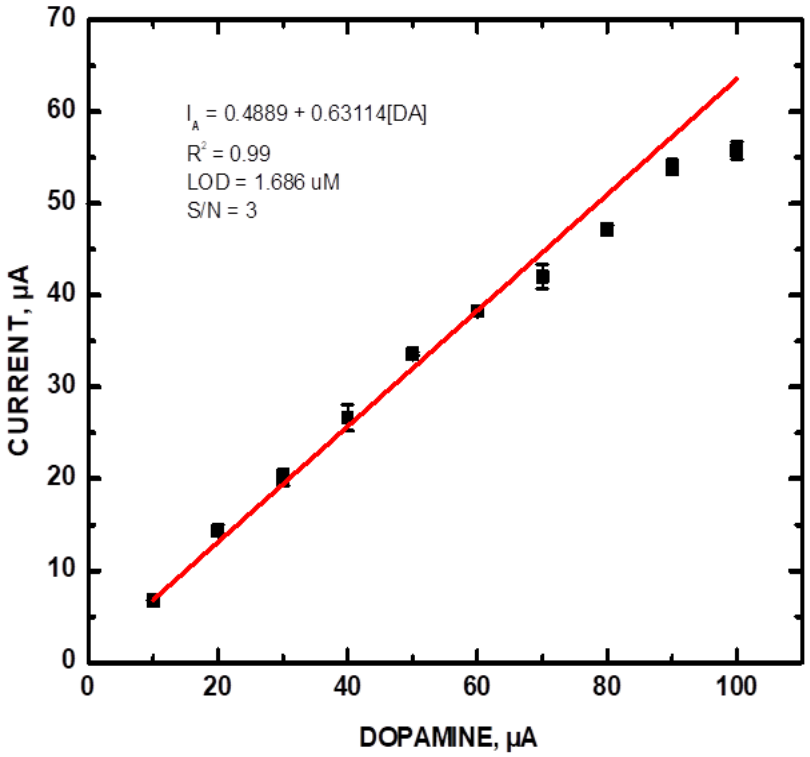

Fig 30. Calibration of SucCDs/Co_3O_4 composite in DA (10-100 µM) in simulated urine

The calibration curve clearly demonstrates that the electrode can effectively detect dopamine concentrations in urine ranging from 10 to 100 µM, with an R^2 value of 0.99. The individual with elevated dopamine levels, due to neuroblastoma, exceeds 10.56 µM, a range within the detectable limit of our developed electrode. Analytically, the limit of detection for our electrode is determined to be 1.686 µM.

SEM image of Co_3O_4-Suc CDs (aggregation seen)

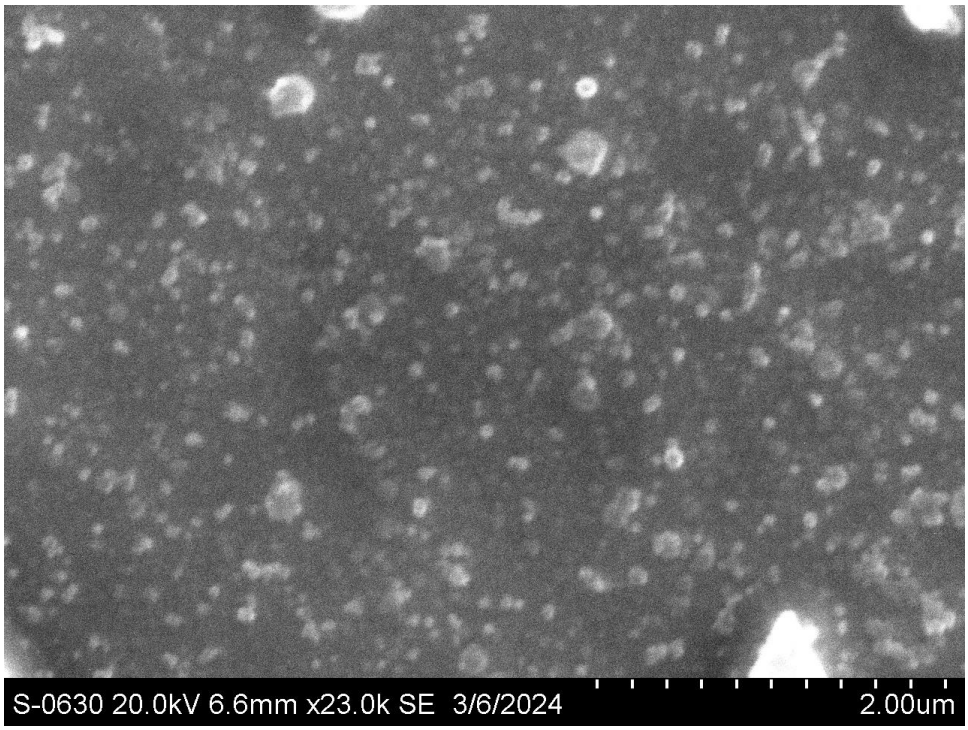

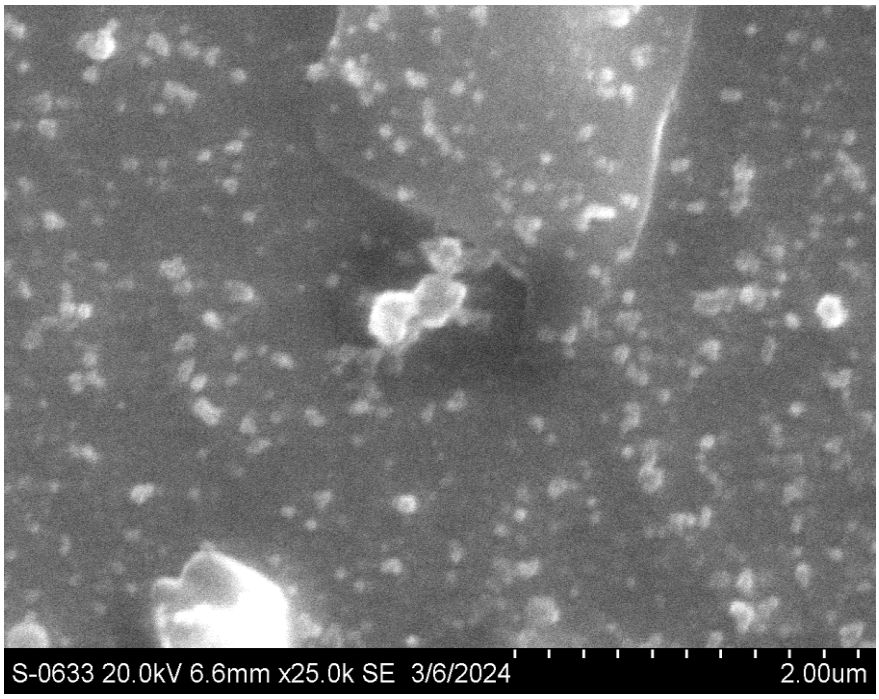

Fig 31. SEM images of Co_3O_4-SucCDs

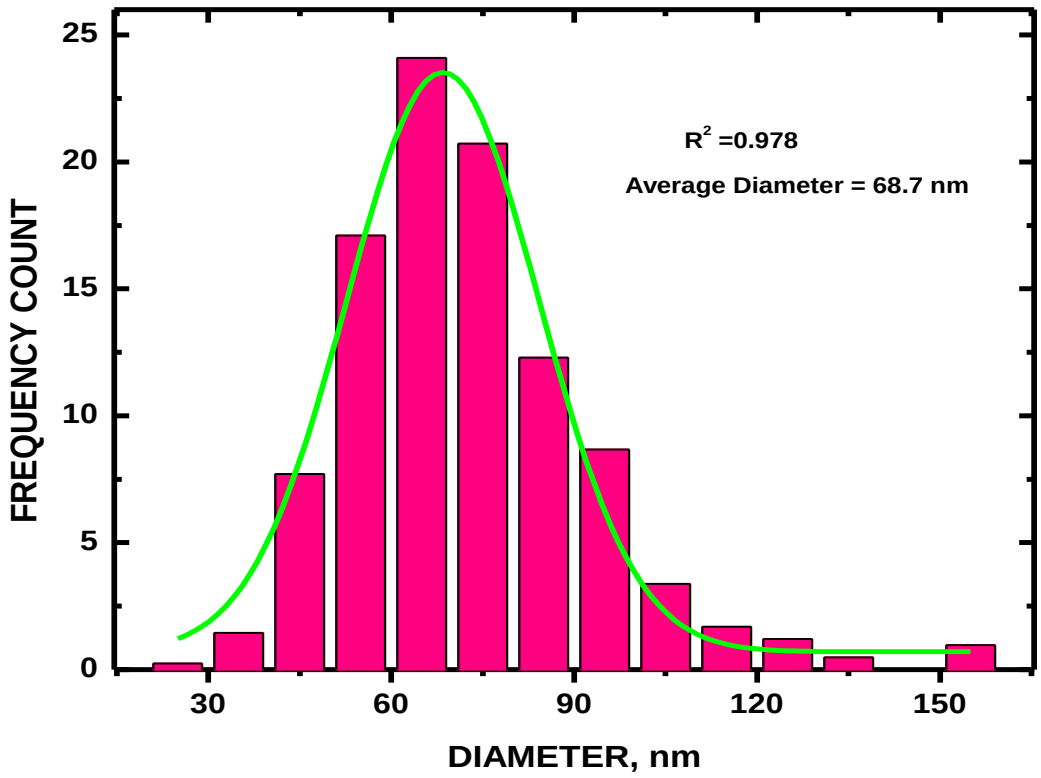

Fig 32. Histogram depicting the size distribution of Co_3O_4 SucCDs composite.

The histogram was generated by analyzing the diameters of particles observed in SEM images using Image J software.

Model	Gauss		
Equation	y=y0 + (A/(w*sqrt(PI/2)))*exp(-2*((x-xc)/w)^2)	**Adjusted R^2 = 0.974**	
Reduced Chi-Sqr	1.73567		
Adj. R-Square	0.97474		
		Value	Standard Error
Relative Frequency	y0	0.70432	0.55012
Relative Frequency	xc	68.47095	0.76989
Relative Frequency	w	31.53547	1.86645
Relative Frequency	A	902.19516	59.61001
Relative Frequency	sigma	15.76773	
Relative Frequency	FWHM	37.13017	
Relative Frequency	Height	22.8266	

Table 2. Particle distribution and their size measurement

SEM-EDX of Co_3O_4-Suc CD (aggregation seen)

Spectrum processing :

Peaks possibly omitted : 2.130, 2.844 keV

Processing option : All elements analyzed (Normalised)

Number of iterations = 5

Standard :

C CaCO3 1-Jun-1999 12:00 AM

O SiO2 1-Jun-1999 12:00 AM

Co Co 1-Jun-1999 12:00 AM

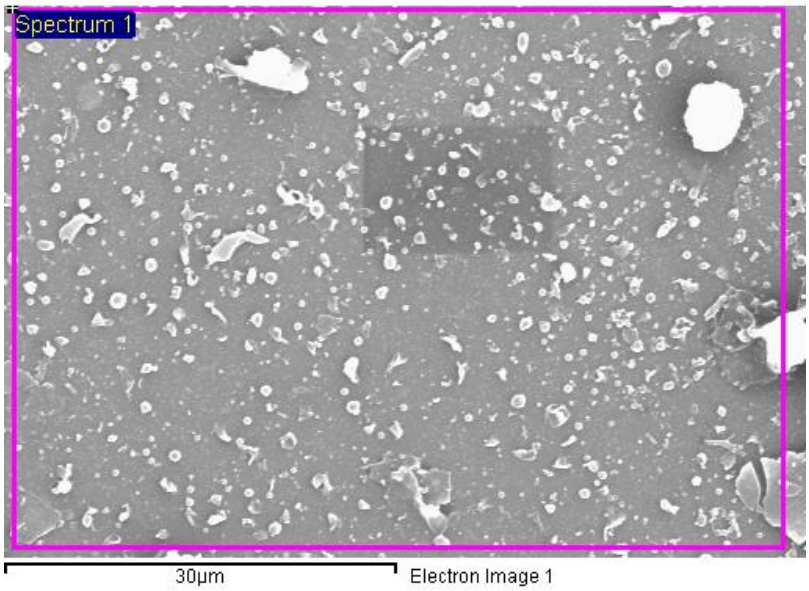

Element	Atomic %
C K	94.86
O K	5.02
Co K	0.13
Total	100

Table 3. EDX report of Co_3O_4-CDs

Totals 100.00

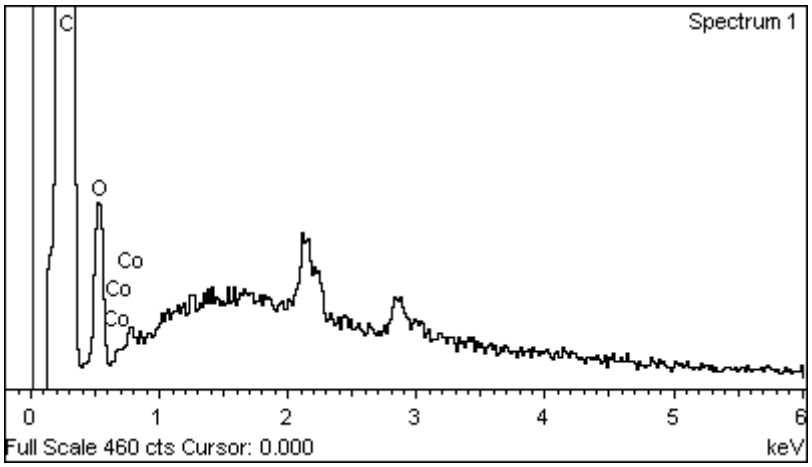

Fig 36. SEM-EDX of Co_3O_4-Suc CD

Coated Co dots lower mag spectrum 1

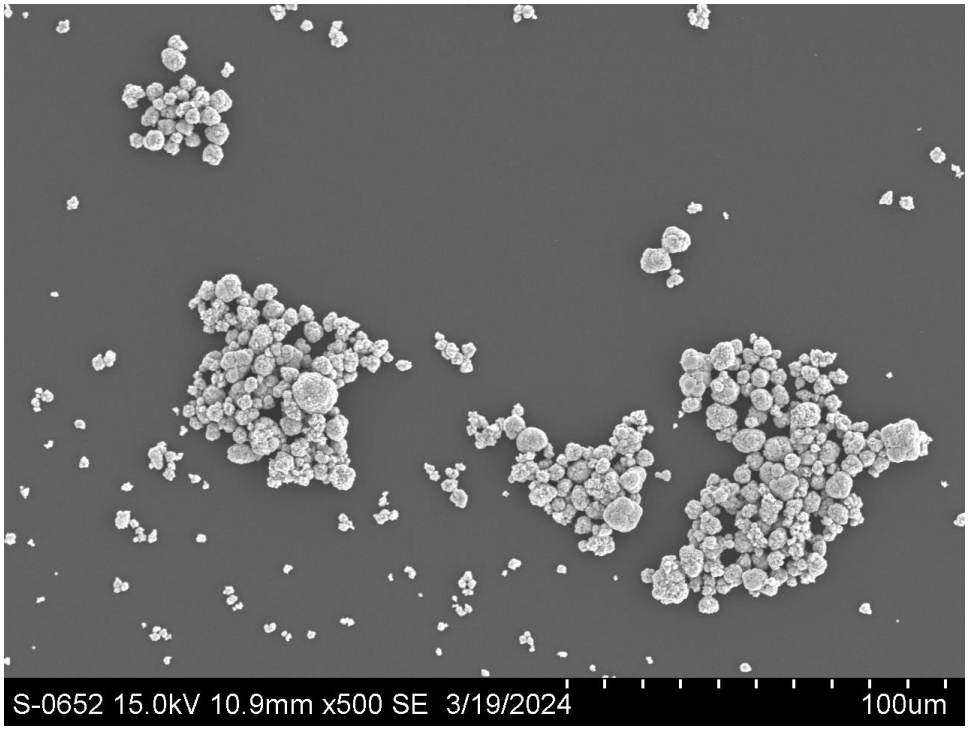

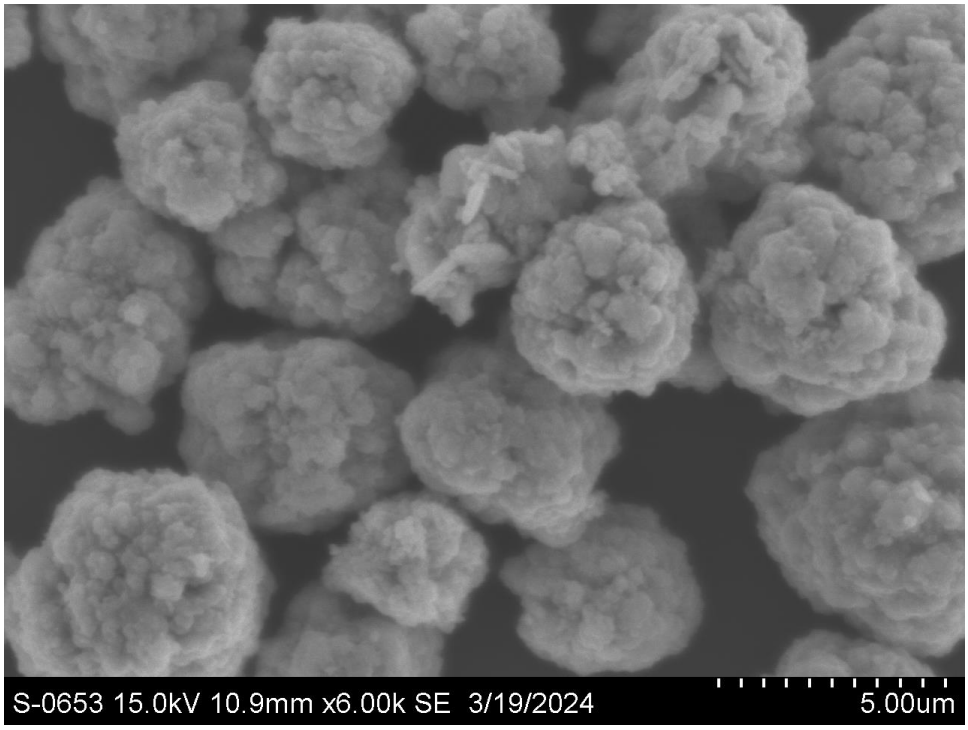

Fig 37. SEM image of Co_3O_4-NPs

Element	Atomic%
C K	43.22
O K	39.10
Co K	16.64
Pd L	0.52
Au M	0.52
Totals	100

Table 4. EDX report of Co_3O_4-CDs

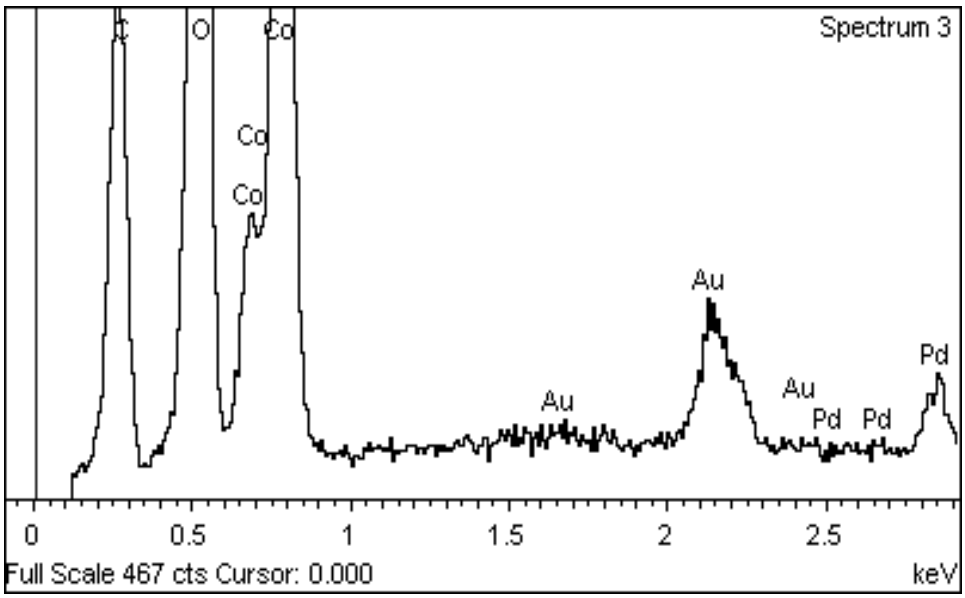

Fig 38. SEM-EDX spectra of coated Co_3O_4 NPs

The detection of cobalt via SEM-EDX is hindered. It is hypothesized that the cobalt presence is masked by a multilayer structure of Suc CDs.

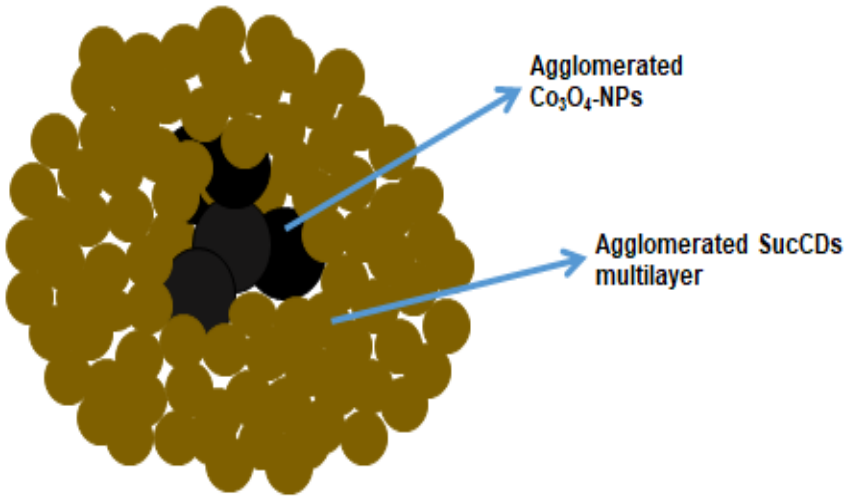

Fig 39. Possible Aggregated seen of Co_3O_4- SucCD

Conclusion

Sucrose-based carbon dots (SucCDs), raffinose-based carbon dots (RafCDs), and palatinose-based carbon dots (PalCDs) were synthesized via a bottom-up hydrothermal approach. Subsequently, a composite of Co_3O_4 and SucCDs was prepared by mixing equal masses of both in 200-proof alcohol followed by 30 minutes of sonication. The resulting Co_3O_4-Suc CDs electrochemical sensor exhibited exceptional sensitivity and selectivity for dopamine detection in simulated urine, as assessed through cyclic voltammetry experiments. The limit of detection of dopamine using the Co_3O_4-SucCDs sensor was determined to be 1.916 µM, with a linear dynamic range of 10-100 µM. Randles-Sevcik analysis indicated that the oxidation of dopamine was diffusion-controlled, with a diffusion coefficient (D) of 5.21×10-5 $cm^2 \cdot s^{-1}$ with R^2 = 0.998. Considering with a 24-hour urination volume of 200 ml, the regular level of dopamine is 400 µg in the total urine. Molarity of dopamine in normal urine = 4.00×10^{-4} g $\frac{1}{189.64} \times \frac{1}{0.2}$ = 10.56 µM which can easily be detected by the electrode. The elevated dopamine level due to neuroblastoma, could be significantly higher than that value.

The study further revealed distinctive integrated Raman peak areas for the D and G bands of SucCDs, PalCDs, and RafCDs, with respective I_D/I_G values of 0.195, 0.117, and 0.0976. The presence of defects in the composite materials notably enhanced sensitivity to dopamine at a potential of +0.2 V which is considered to be close to the Fermi level. The agglomeration of carbon dots (CDs) was seen. Calibration of dopamine detection exhibited a linear relationship (i_P = 0.0696 [DA] + 25.6) within the concentration range of 10 to 100 µM, demonstrating selectivity against interfering substances such as uric acid, glucose, urea, and ascorbic acid. Incorporation of Co_3O_4 nanoparticles (NPs) significantly reduced

the detection limit of dopamine in simulated urine to 1.916 µM, with R^2 = 0.99 within the dynamic range of 10-100 µM. SEM-EDX analysis and using image J software, average composite particle size was calculated as 68.47 nm ±0.769 with a 0.6% cobalt content, although the actual percentage of Co detected might be lower due to the formation of multilayers of CDs around Co_3O_4.

References

1. Liu, Junjun, Rui Li, and Bai Yang. "Carbon Dots: A New Type of Carbon-Based Nanomaterial with Wide Applications." *ACS Central Science* 6, no. 12 (December 23, 2020): 2179–95. https://doi.org/10.1021/acscentsci.0c01306.
2. Gaur, M., Misra, C., Yadav, A. B., Swaroop, S., Maolmhuaidh, F. Ó., Bechelany, M., & Barhoum, A. Biomedical Applications of Carbon Nanomaterials: Fullerenes, Quantum Dots, Nanotubes, Nanofibers, and Graphene. *Materials*, *14*(20), 5978. https://doi.org/10.3390/ma14205978
3. Banhart, Florian, Jani Kotakoski, and Arkady V. Krasheninnikov. "Structural Defects in Graphene." *ACS Nano* 5, no. 1 (January 25, 2011): 26–41. https://doi.org/10.1021/nn102598m.
4. Tu, Qiang, and Chang Chang. "Diagnostic Applications of Raman Spectroscopy." *Nanomedicine: Nanotechnology, Biology and Medicine* 8, no. 5 (July 2012): 545–58. https://doi.org/10.1016/j.nano.2011.09.013.
5. Martinez, Lourdes, and Lili He. "Detection of Mycotoxins in Food Using Surface-Enhanced Raman Spectroscopy: A Review." *ACS Applied Bio Materials* 4, no. 1 (January 18, 2021): 295–310. https://doi.org/10.1021/acsabm.0c01349.

6. Puchowicz, Dorota, Patrycja Giesz, Marcin Kozanecki, and Małgorzata Cieślak. “Surface-Enhanced Raman Spectroscopy (SERS) in Cotton Fabrics Analysis.” *Talanta* 195 (April 2019): 516–24. https://doi.org/10.1016/j.talanta.2018.11.059.
7. Desroches, Joannie, Michael Jermyn, Michael Pinto, Fabien Picot, Marie-Andrée Tremblay, Sami Obaid, Eric Marple, et al. “A New Method Using Raman Spectroscopy for in Vivo Targeted Brain Cancer Tissue Biopsy.” *Scientific Reports* 8, no. 1 (January 29, 2018): 1792. https://doi.org/10.1038/s41598-018-20233-3.
8. Menżyk, Alicja, Alessandro Damin, Agnieszka Martyna, Eugenio Alladio, Marco Vincenti, Gianmario Martra, and Grzegorz Zadora. “Toward a Novel Framework for Bloodstains Dating by Raman Spectroscopy: How to Avoid Sample Photodamage and Subsampling Errors.” *Talanta* 209 (March 2020): 120565. https://doi.org/10.1016/j.talanta.2019.120565.
9. Geraldes, Carlos F. G. C. “Introduction to Infrared and Raman-Based Biomedical Molecular Imaging and Comparison with Other Modalities.” *Molecules* 25, no. 23 (November 26, 2020): 5547. https://doi.org/10.3390/molecules25235547.
10. Cançado, L. G., A. Jorio, E. H. Martins Ferreira, F. Stavale, C. A. Achete, R. B. Capaz, M. V. O. Moutinho, A. Lombardo, T. S. Kulmala, and A. C. Ferrari. “Quantifying Defects in Graphene via Raman Spectroscopy at Different Excitation Energies.” *Nano Letters* 11, no. 8 (August 10, 2011): 3190–96. https://doi.org/10.1021/nl201432g
11. Hull, Robert V., Liang Li, Yangchuan Xing, and Charles C. Chusuei. “Pt Nanoparticle Binding on Functionalized Multiwalled Carbon Nanotubes.” *Chemistry of Materials* 18, no. 7 (April 1, 2006): 1780–88. https://doi.org/10.1021/cm0518978.
12. Eckmann, Axel, Alexandre Felten, Artem Mishchenko, Liam Britnell, Ralph Krupke, Kostya S. Novoselov, and Cinzia Casiraghi. “Probing the Nature of Defects in Graphene by Raman Spectroscopy.” *Nano Letters* 12, no. 8 (August 8, 2012): 3925–30. https://doi.org/10.1021/nl300901a.

13. Eckmann, A.; Felten, A.; Mishchenko, A.; Britnell, L.; Krupke, R.; Novoselov, K. S.; Casiraghi, C. Probing the Nature of Defects in Graphene by Raman Spectroscopy. *Nano Lett.* **2012**, *12*, 3925– 3930, DOI: 10.1021/nl300901a.
14. Lucchese, M. M.; Stavale, F.; Ferreira, E. H. M.; Vilani, C.; Moutinho, M. V. O.; Capaz, R. B.; Achete, C. A.; Jorio, A. Quantifying Ion-Induced Defects and Raman Relaxation Length in Graphene. *Carbon* **2010**, *48*, 1592– 1597, DOI: 10.1016/j.carbon.2009.12.057
15. Puech, P.; Kandara, M.; Paredes, G.; Moulin, L.; Weiss-Hortala, E.; Kundu, A.; Ratel-Ramond, N.; Plewa, J.-M.; Pellenq, R.; Monthioux, M. Analyzing the Raman Spectra of Graphenic Carbon Materials from Kerogens to Nanotubes: What Type of Information Can Be Extracted from Defect Bands?. *C — J. Carbon Res.* **2019**, *5*, 69, DOI: 10.3390/c5040069
16. Gupta, A. K.; Nisoli, C.; Lammert, P. E.; Crespi, V. H.; Eklund, P. C. Curvature-Induced D-Band Raman Scattering in Folded Graphene. *J. Phys.: Condens. Matter* **2010**, *22*, 334205, DOI: 10.1088/0953-8984/22/33/334205
17. Picheau, Emmanuel, Anthony Impellizzeri, Dmitry Rybkovskiy, Maxime Bayle, Jean-Yves Mevellec, Ferdinand Hof, Hassan Saadaoui, et al. "Intense Raman D Band without Disorder in Flattened Carbon Nanotubes." *ACS Nano* 15, no. 1 (January 26, 2021): 596–603. https://doi.org/10.1021/acsnano.0c06048.
18. Xu, X.; Ray, R.; Gu, Y.; Ploehn, H. J.; Gearheart, L.; Raker, K.; Scrivens, W. A. J Am Chem Soc 2004, 126, 12736-12737.
19. Yang, Y.; Ji, X.; Jing, M.; Hou, H.; Zhu, Y.; Fang, L.; Yang, X.; Chen, Q.; Banks, C. E. J Mater Chem A 2015, 3, 5648-5655.
20. Wu, Z. L.; Zhang, P.; Gao, M. X.; Liu, C. F.; Wang, W.; Leng, F.; Huang, C. Z. J Mater Chem B 2013, 1, 2868.
21. Zhu, S.; Meng, Q.; Wang, L.; Zhang, J.; Song, Y.; Jin, H.; Zhang, K.; Sun, H.;

Wang, H.; Yang, B. Angew Chem 2013, 125, 4045-4049

22. Jiang, K.; Sun, S.; Zhang, L.; Lu, Y.; Wu, A.; Cai, C.; Lin, H. Angew Chem Int Ed 2015, 54, 5360-5363

23. Baker, S. N.; Baker, G. A. Angew Chem Int Ed 2010, 49, 6726-6744.

24. Qiu, Jianrong, Yang Li, and Yongchao Jia. "Synthesis Methods." In *Persistent Phosphors*, 31–67. Elsevier, 2021. https://doi.org/10.1016/B978-0-12-818637-4.00002-1.

25. Huang, Guoming, Chun-Hua Lu, and Huang-Hao Yang. "Magnetic Nanomaterials for Magnetic Bioanalysis." In *Novel Nanomaterials for Biomedical, Environmental and Energy Applications*, 89–109. Elsevier, 2019. https://doi.org/10.1016/B978-0-12-814497-8.00003-5

26. Arcudi, Francesca, Luka Đorđević, and Maurizio Prato. "Design, Synthesis, and Functionalization Strategies of Tailored Carbon Nanodots." *Accounts of Chemical Research* 52, no. 8 (August 20, 2019): 2070–79. https://doi.org/10.1021/acs.accounts.9b00249

27. Nguyen, V.-T.; Kwon, Y. S.; Gu, M. B. Aptamer-based environmental biosensors for molecule contaminants. *Curr. Opin. Biotechnol.* **2017**, *45*, 15– 23, DOI: 10.1016/j.copbio.2016.11.020

28. Mansuriya, Bhargav D., and Zeynep Altintas. "Carbon Dots: Classification, Propertie Synthesis, Characterization, and Applications in Health Care—An Updated Review (2018–2021)." *Nanomaterials* 11, no. 10 (September 27, 2021): 2525. https://doi.org/10.3390/nano11102525

29. Ross, Sukunya, Ren-Siang Wu, Shih-Chun Wei, Gareth M Ross, and Huan-Tsung Chang. "The Analytical and Biomedical Applications of Carbon Dots and Their Future Theranostic Potential: A Review." *Journal of Food and Drug Analysis* 28, no. 4 (December 2, 2020): 678–96. https://doi.org/10.38212/2224-6614.1154.

30. Griesche, C.; Baeumner, A. J. Biosensors to support sustainable agriculture and food safety. *TrAC, Trends Anal. Chem.* **2020**, *128*, 115906, DOI: 10.1016/j.trac.2020.115906

31. Smart, A., A. Crew, R. Pemberton, G. Hughes, O. Doran, and J.P. Hart. "Screen-Printed Carbon Based Biosensors and Their Applications in Agri-Food Safety." *TrAC Trends in Analytical Chemistry* 127 (June 2020): 115898. https://doi.org/10.1016/j.trac.2020.115898.

32. Xu, X. Y.; Ray, R.; Gu, Y. L.; Ploehn, H. J.; Gearheart, L.; Raker, K.; Scrivens, W. A. Electrophoretic analysis and purification of fluorescent single-walled carbon nanotube fragments. *J. Am. Chem. Soc.* **2004**, *126*, 12736– 12737, DOI: 10.1021/ja040082h

33. Jiang, Y.; Shi, M.; Liu, Y.; Wan, S.; Cui, C.; Zhang, L.; Tan, W. Aptamer/AuNP biosensor for colorimetric profiling of exosomal proteins. *Angew. Chem., Int. Ed.* **2017**, *56*, 1191611920, DOI: 10.1002/anie.201703807

34. Zou, S.; Huang, S.; Li, Y.; Zhao, N.; Li, H.; Angelidaki, I.; Zhang, Y. Microbial fuel cell-based, biosensor for toxic carbon monoxide monitoring. *Talanta* **2018**, *186*, 368– 371 DOI: 10.1016/j.talanta.2018.04.084

35. Liu, Junjun, Rui Li, and Bai Yang. "Carbon Dots: A New Type of Carbon-Based Nanomaterial with Wide Applications." *ACS Central Science* 6, no. 12 (December 23, 2020): 2179–95. https://doi.org/10.1021/acscentsci.0c01306.

36. Elugoke, Saheed E., Omolola E. Fayemi, Abolanle S. Adekunle, Bhekie B. Mamba, Thabo T. I. Nkambule, and Eno E. Ebenso. "Electrochemical Sensor for the detection of Dopamine Using Carbon Quantum Dots/Copper Oxide Nano composite modified Electrode." *FlatChem* 33 (2022): 100372. https://doi.org/10.1016/j.flatc.2022.100372.

37. M.Jr. Bruchez, M. Moronne, P. Gin, S. Weiss, A.P. Alivisatos Semiconductor nanocrystals as fluorescent biological labels Science, 281 (1998), pp. 2013-2016

38. Mathieu P, Favrot M, Frappaz D, Chauvin F, Greffe J, Montegue A, Lacroix C, David L, Brunat- expérience de dépistage en France [Neuroblastoma in children: clinical and biological aspects An experience of screening in France]. Ann Biol Clin (Paris). 1993; 51(7- 8):665-88. French PMID: 8166384

39. M.Jr. Bruchez, M. Moronne, P. Gin, S. Weiss, A.P. Alivisatos Semiconductor nanocrystals as fluorescent biological labels Science, 281 (1998), pp. 2013-2016.

40. A. Valizadeh, H. Mikaeili, M. Samiei, S.M. Farkhani, N. Zarghami, M. Kouhi, A. Akbarzadeh, S. Davaran Quantum dots: synthesis, bioapplications, and toxicity Nanoscale Res. Lett., 7 (2012), p. 480 29. N. Wei, X. E. Zhao, S. Y. Zhu, Y. R. He, L. F. Zheng, G. Chen, J. M. You, S. Liu, Z. Q. Liu, *Talanta* 2016, 161, 253

41. Liu, Xixia, and Juewen Liu. "Biosensors and Sensors for Dopamine Detection." *VIEW* 2, no. 1 (February 2021): 20200102. https://doi.org/10.1002/VIW.20200102

42. Elgrishi, Noémie, Kelley J. Rountree, Brian D. McCarthy, Eric S. Rountree, Thomas T. Eisenhart, and Jillian L. Dempsey. "A Practical Beginner's Guide to Cyclic voltammetry" *Journal of Chemical Education* 95, no. 2 (February 13, 2018): 197–206. https://doi.org/10.1021/acs.jchemed.7b00361.

43. Seven, Elif S., Shiv K. Sharma, Dihya Meziane, Yiqun Zhou, Keenan J. Mintz, Raja R. Pandey, Charles C. Chusuei, and Roger M. Leblanc. "Close-Packed Langmuir Monolayers of Saccharide-Based Carbon Dots at the Air–Subphase Interface. *Langmuir* 35, no. 20 (May 21, 2019): 6708–18. https://doi.org/10.1021/acs.langmuir.9b00920.

44. A. Madalena CC, S. Kenichi, C. Richard G. Voltammetric detection of glutathione: an adsorptive stripping voltammetry approach. Analyst, 2016, 141(10), 2904-2910.

45. Chusuei, Charles C., and Ram Chandra Nepal. "Role of Defects and Exposed Graphene in Carbon Nanomaterial-Based Electrocatalysts." *New Journal of Chemistry* 48, no. 1 (2024): 260– 67. https://doi.org/10.1039/D3NJ04054B

46. Kislenko, Vitaliy A., Sergey V. Pavlov, and Sergey A. Kislenko. "Influence of Defects in Grapheme on Electron Transfer Kinetics: The Role of the Surface Electronic Structure." *Electrochimica Acta* 341 (May 2020): 136011. https://doi.org/10.1016/j.electacta.2020.136011

47. Kader, Mohammad S., and Charles C. Chusuei. “A Cobalt (II) Oxide Carbon Nanotube Composite to Assay Dopamine.” *Chemosensors* 8, no. 2 (March 25,2020): 22. https://doi.org/10.3390/chemosensors8020022.

48. Chusuei, C. C.; Clark, C. J.; Pandey, R. R.; Williams, E. T.; Shuxteau, C.; Seven, E. S.; Leblanc, R. M. Graphene Defects in Saccharide Carbon Dots Govern Electrochemical Sensitivity. *Electroanalysis* **2021**, *33* (11), 2261–2266. https://doi.org/10.1002/elan.202100381.

49. Zanello, P. Inorganic Electrochemistry: *Theory, Practice and Applications; Royal Society of Chemistry: Cambridge, 2003.*

50. Karki, Nawaraj, Albert V. Davydov, Sergiy Krylyuk, and Charles C. Chusuei. “Electrochemically Assaying Dopamine with P-Doped Silicon Nanowires.” *Analytica Letters* 55, no. 14 (September 22, 2022): 2161–69. https://doi.org/10.1080/00032719.2022.2048845.

51. Henry, John Bernard. Henry’s Clinical Diagnosis and Management by Laboratory Methods. Edited by Richard A. McPherson and Matthew R. Pincus. Twenty-Fourth edition. Amsterdam: Elsevier, 2021.

Appendix A

SEM images of Co_3O_4 – Suc CDs

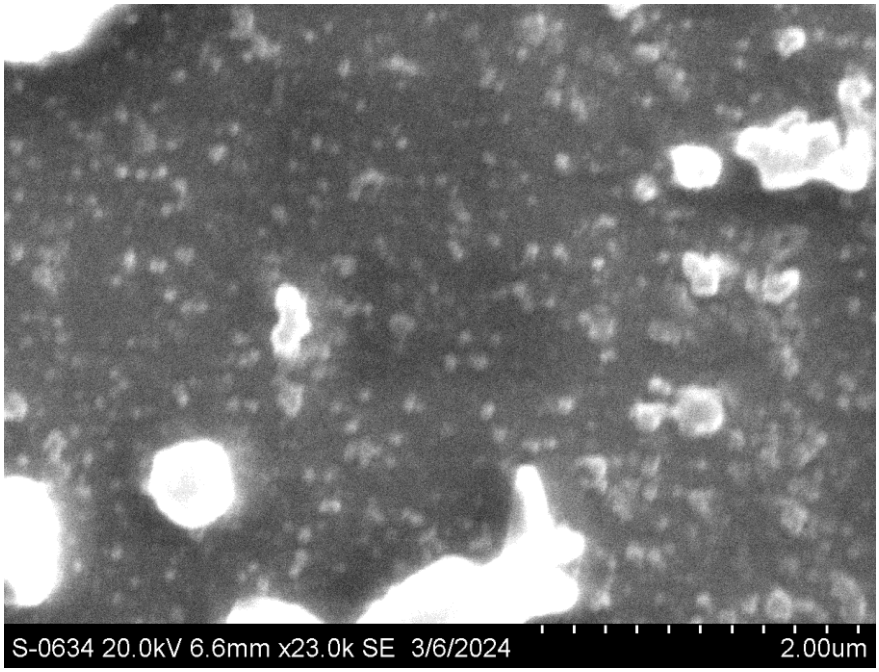

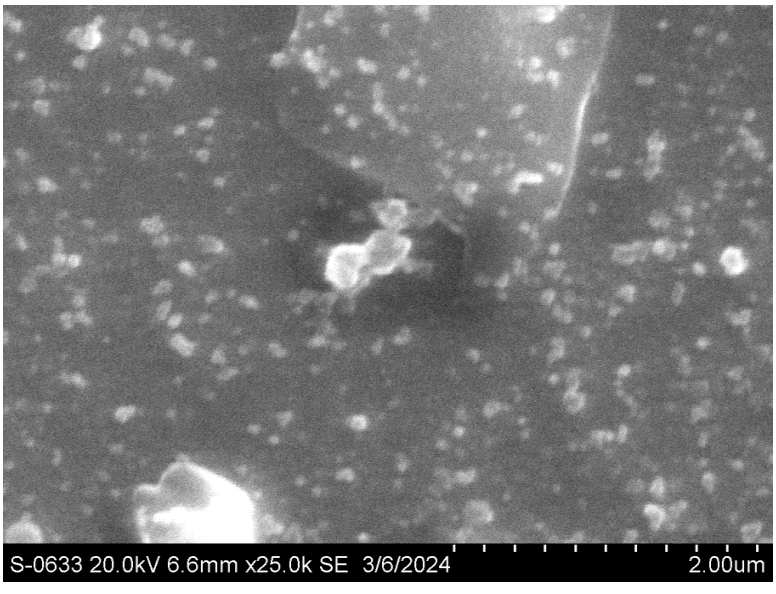

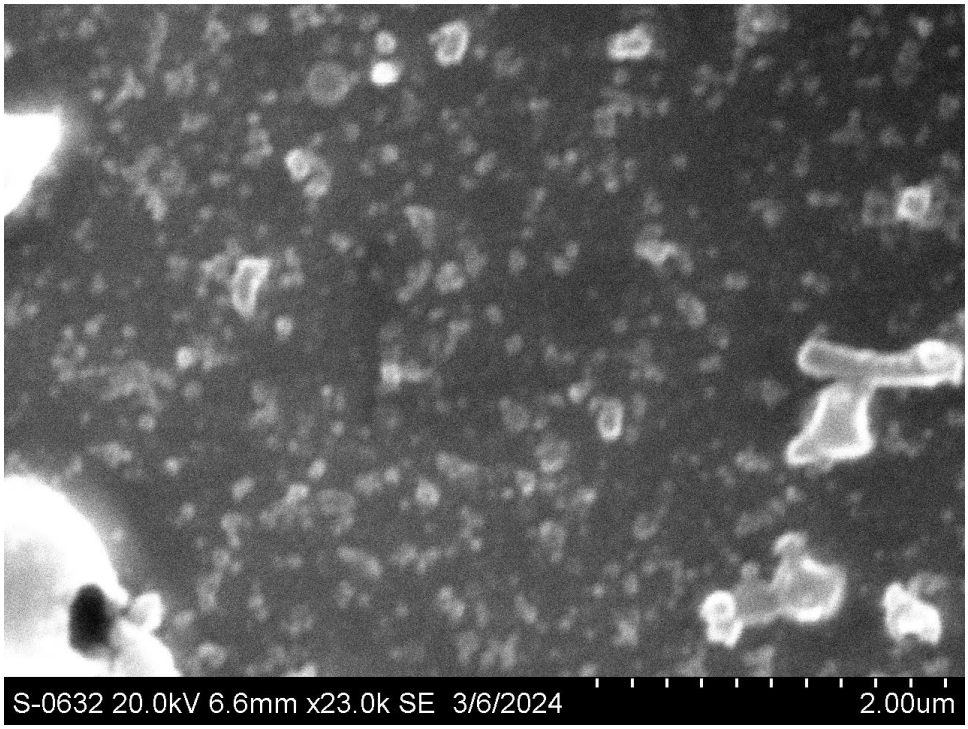

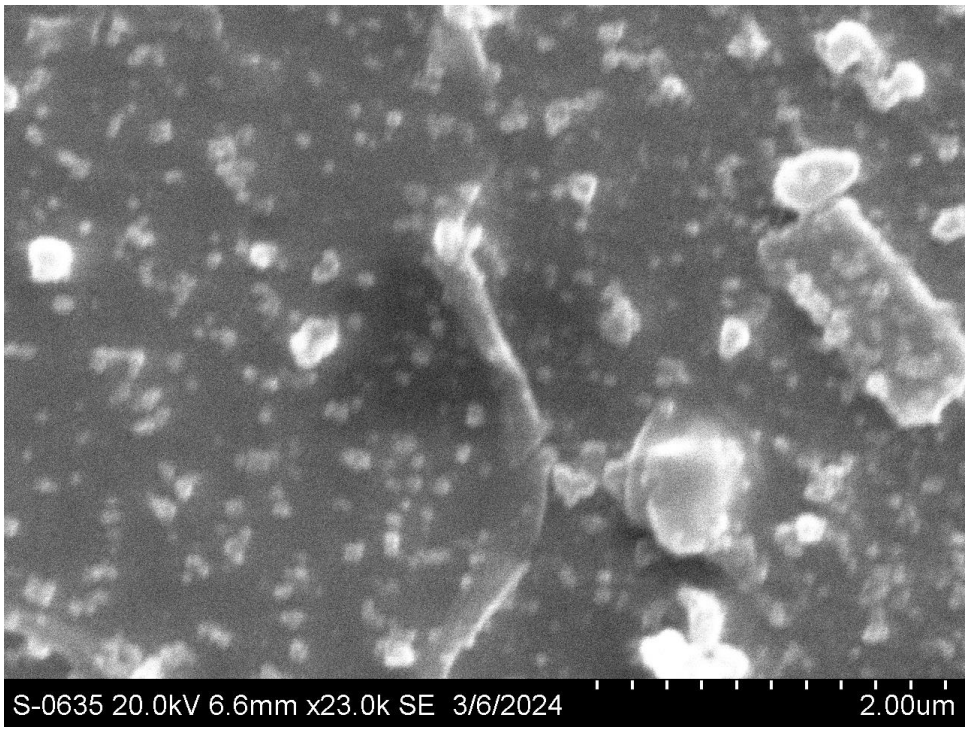

Fig 32. SEM images of Co_3O_4- Suc CD

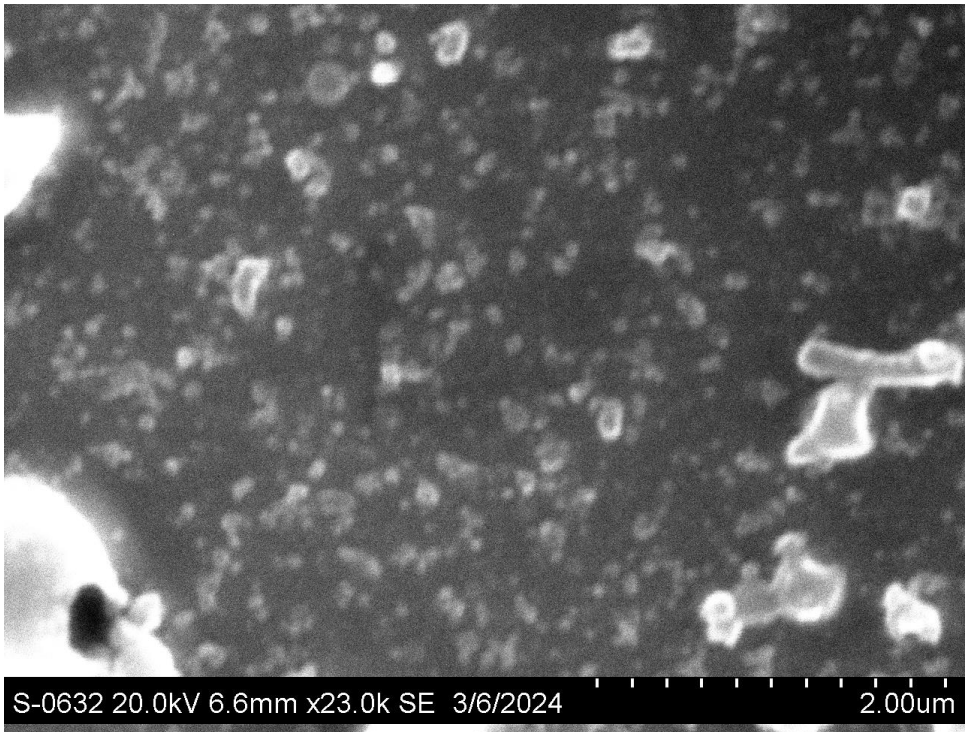
S-0632 20.0kV 6.6mm x23.0k SE 3/6/2024
2.00um

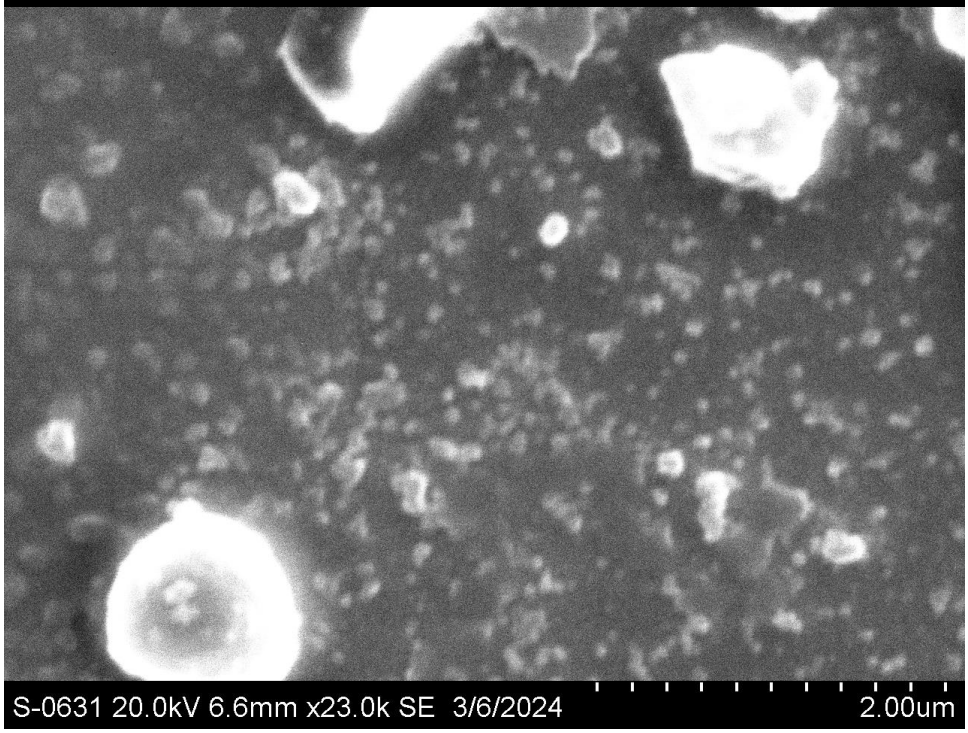
S-0631 20.0kV 6.6mm x23.0k SE 3/6/2024
2.00um

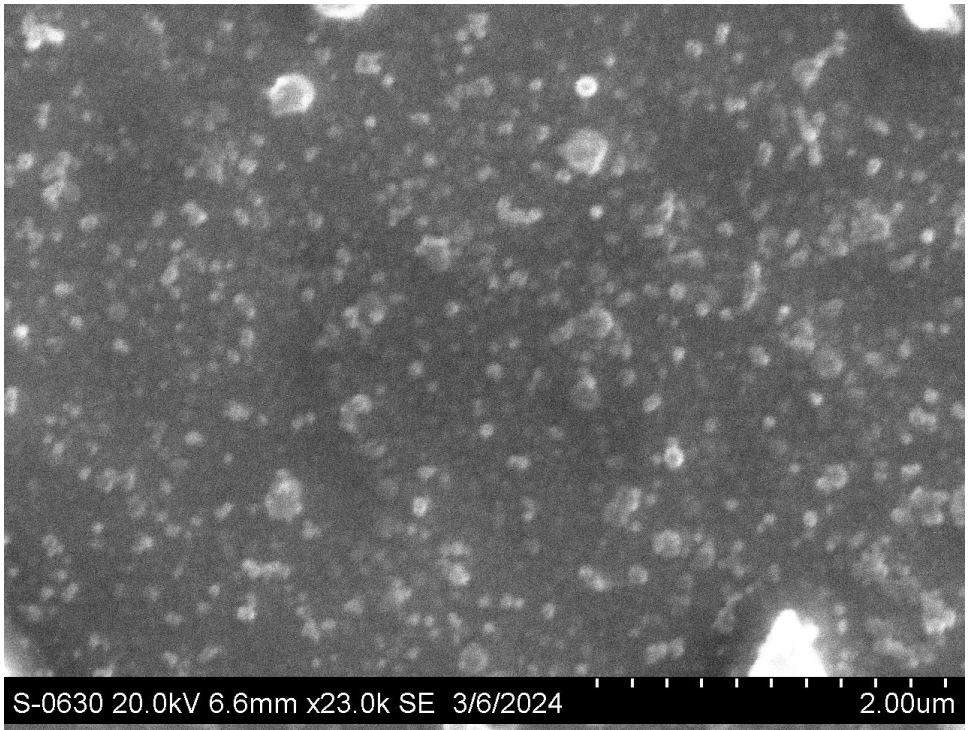

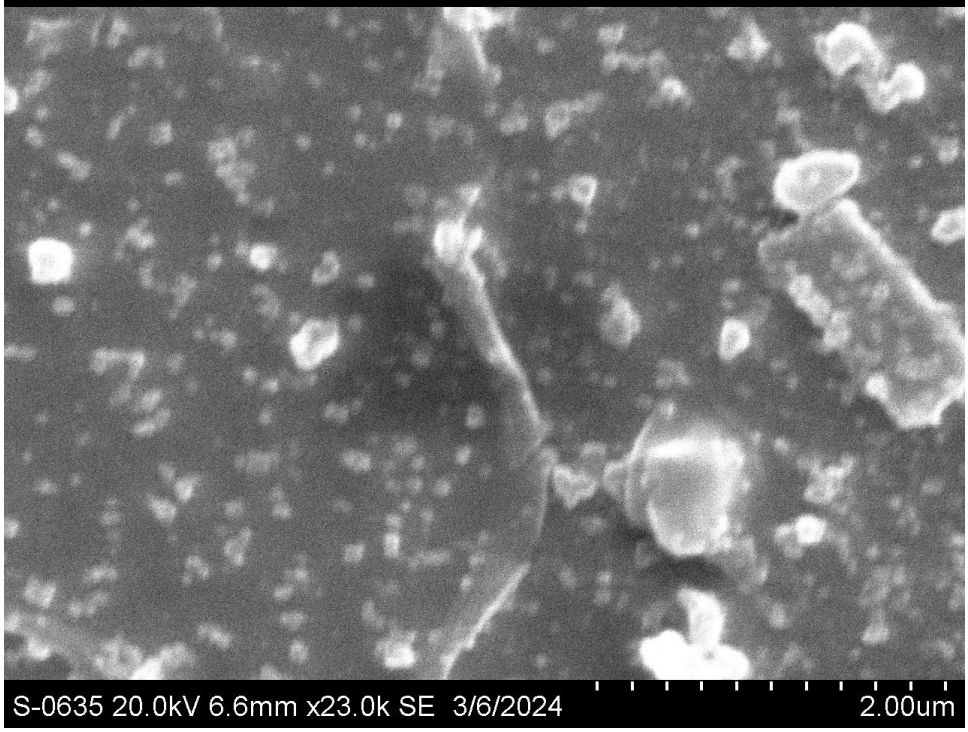

Magnifying SEM image shows the strange micron size particles. To confirm there is no impurities,

EDX analysis was done.

SucroSucrose dots EDX spectrum 1

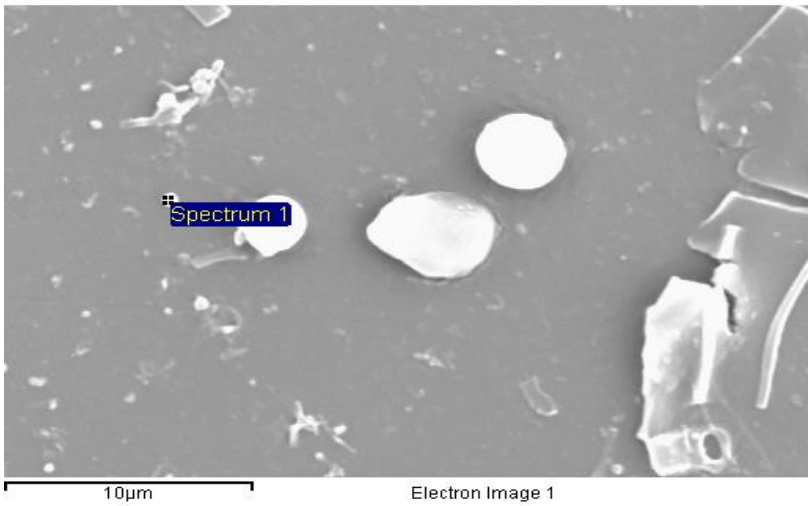

Spectrum processing :

Peak possibly omitted : 1.050 keV

Processing option : All elements analyzed (Normalised)

Number of iterations = 3

Standard :

C CaCO3 1-Jun-1999 12:00 AM

O SiO2 1-Jun-1999 12:00 AM

Pd Pd 1-Jun-1999 12:00 AM

Au Au 1-Jun-1999 12:00 AM

Element	Weight%	Atomic%
C K	83.29	91.08
O K	10.17	8.35
Pd L	2.34	0.29
Au M	4.20	0.28
Totals	100.00	

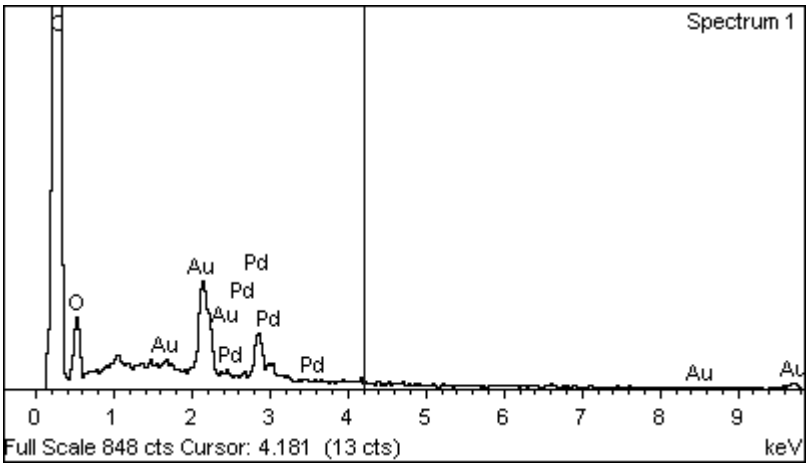

Coated Co_3O_4-CDs dots spectrum 2

Spectrum processing:

Peaks possibly omitted: 2.130, 2.850, 3.032 keV

Processing option : All elements analyzed (Normalised)

Number of iterations = 4

Standard :

C CaCO3 1-Jun-1999 12:00 AM

O SiO2 1-Jun-1999 12:00 AM

Co Co 1-Jun-1999 12:00 AM

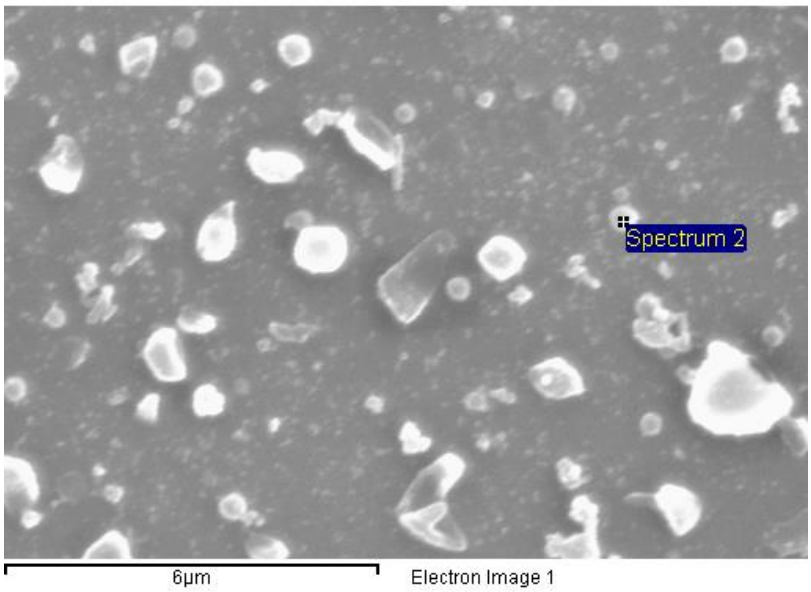

Element	Weight%	Atomic%
C K	95.60	96.68
O K	4.36	3.31
Co K	0.04	0.01
Totals	100.00	

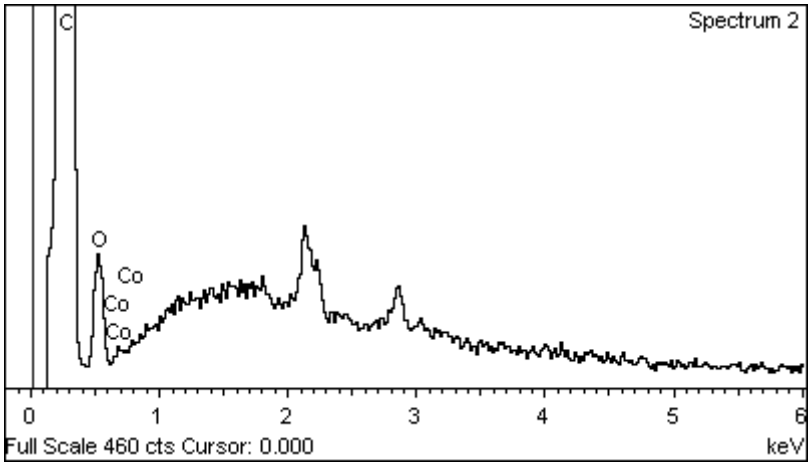

Coated Co_3O_4-CDs spectrum 5

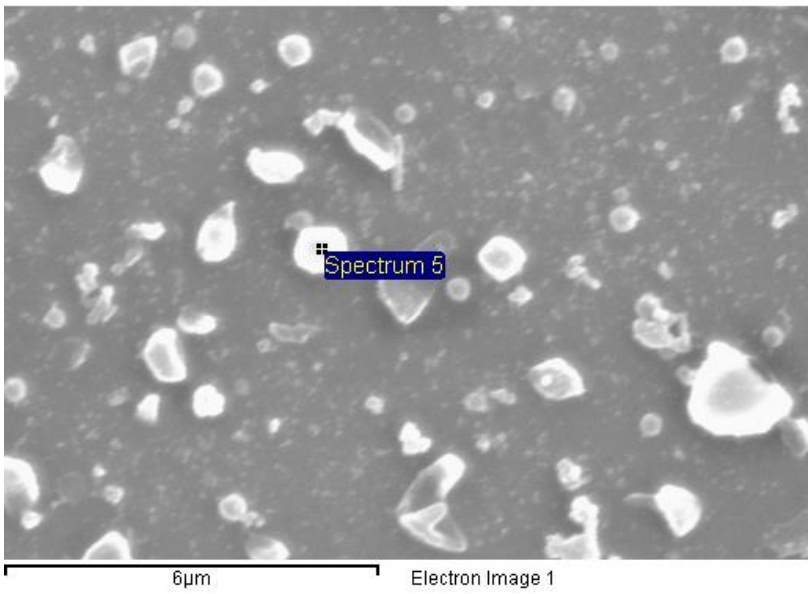

Spectrum processing :

Peaks possibly omitted : 2.138, 2.845 keV

Processing option : All elements analyzed (Normalised)

Number of iterations = 4

Standard :

C CaCO3 1-Jun-1999 12:00 AM

O SiO2 1-Jun-1999 12:00 AM

Co Co 1-Jun-1999 12:00 AM

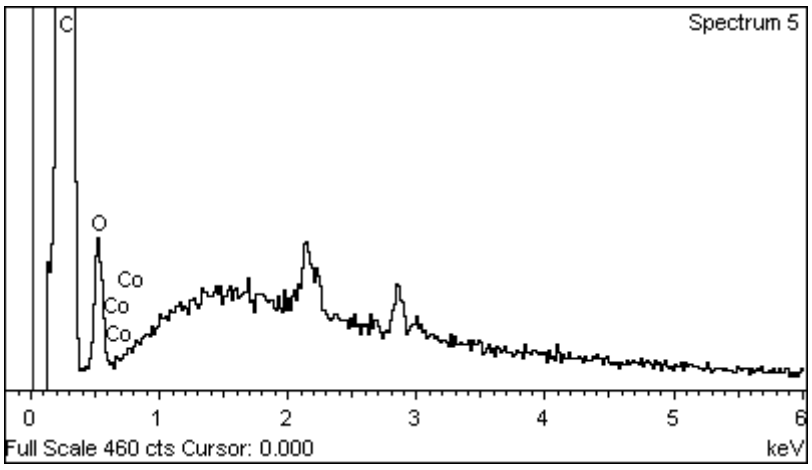

Element	Weight%	Atomic%
C K	95.45	96.57
O K	4.51	3.43
Co K	0.03	0.01
Total	100	

Sucrose dots EDX spectrum 2

Spectrum processing:

No peaks omitted

Processing option : All elements analyzed (Normalised)

Number of iterations = 3

Standard :

C CaCO3 1-Jun-1999 12:00 AM

O SiO2 1-Jun-1999 12:00 AM

Na Albite 1-Jun-1999 12:00 AM

Pd Pd 1-Jun-1999 12:00 AM

Au Au 1-Jun-1999 12:00 AM

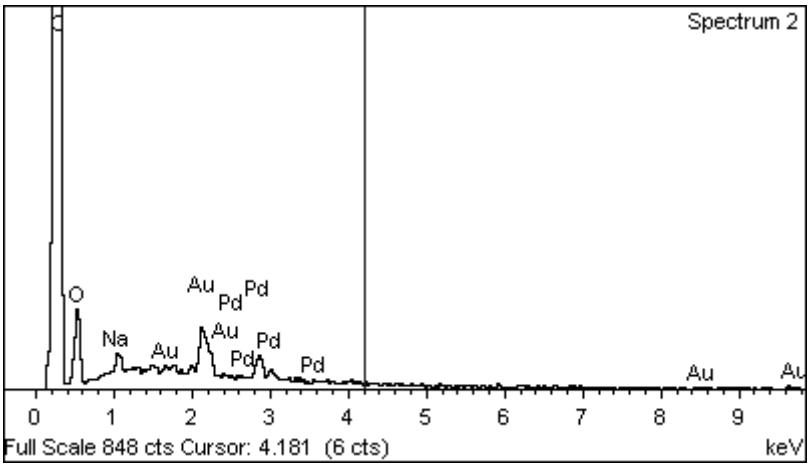

Element	Weight%	Atomic%
C K	83.42	89.65
O K	12.19	9.83
Na K	0.30	0.17
Pd L	1.50	0.18
Au M	2.60	0.17
Totals	100.00	

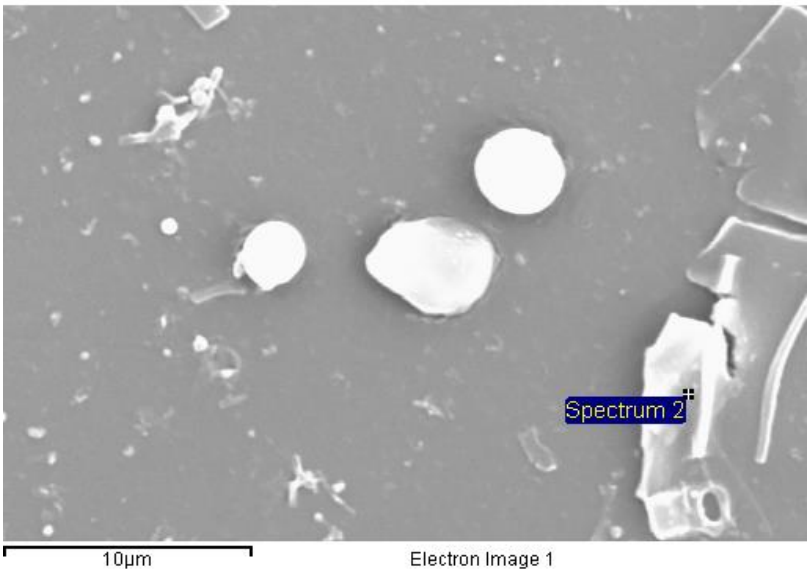

EDX analysis of Suc-CDs

In Table 1 EDX revealed that 91.08 atomic % of carbon and 8.35 atomic % of oxygen. The palladium and the gold appeared in lower atomic % is due to the coating of sample during SEM experiment. In electron microscopy, coating to samples is essential to enhance their image quality. By depositing a metal conductive layer on the sample, it prevents charging, minimizes thermal damage, and enhances the secondary electron signal.

XRF analysis of composite Co_3O_4-SucCDs

X-ray Fluorescence (XRF) is an analytical technique that uses the interaction of X-rays with a sample to determine its elemental composition. XRF has a greater capability to detect metals through deeper penetration compared to energy-dispersive X-ray spectroscopy EDX. While EDX failed to detect cobalt in the composite it was successfully identified using XRF in this instance.

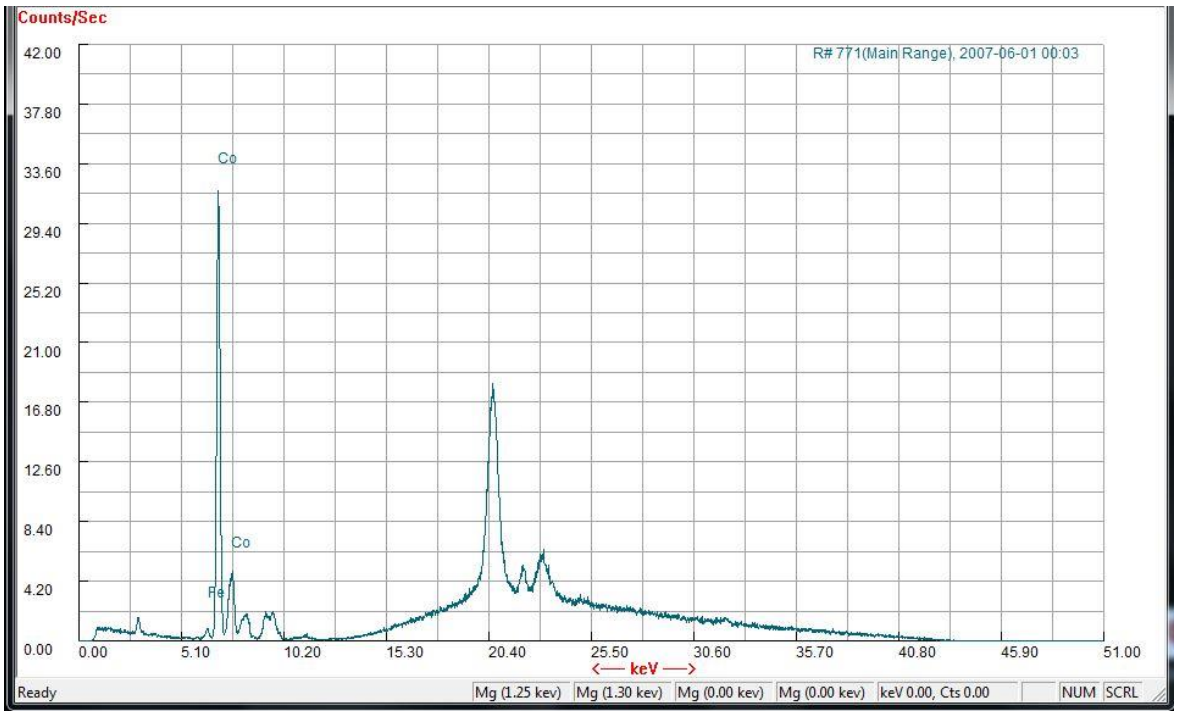

Fig. XRF spectra for Co_3O_4-SucCDs

Appendix B – Additional CV data

Comparison of Fru-CDs, Raf-CDs, Pal-CDs, Gal-CDs and Suc-CDs for their utility in acetaminophen sensing

Acetaminophen (APAP) is an antipyretic analgesic drug and can be purchased without prescription. Continuous real-time monitoring of APAP in clinical settings is crucial for preventing liver toxicity resulting from accidental overdose of the APAP. Galactose carbon dots were identified as the most effective for electrochemical sensing of acetaminophen. The study investigated the correlation between the graphene defect density of carbon dots and their electrochemical sensing properties for APAP.

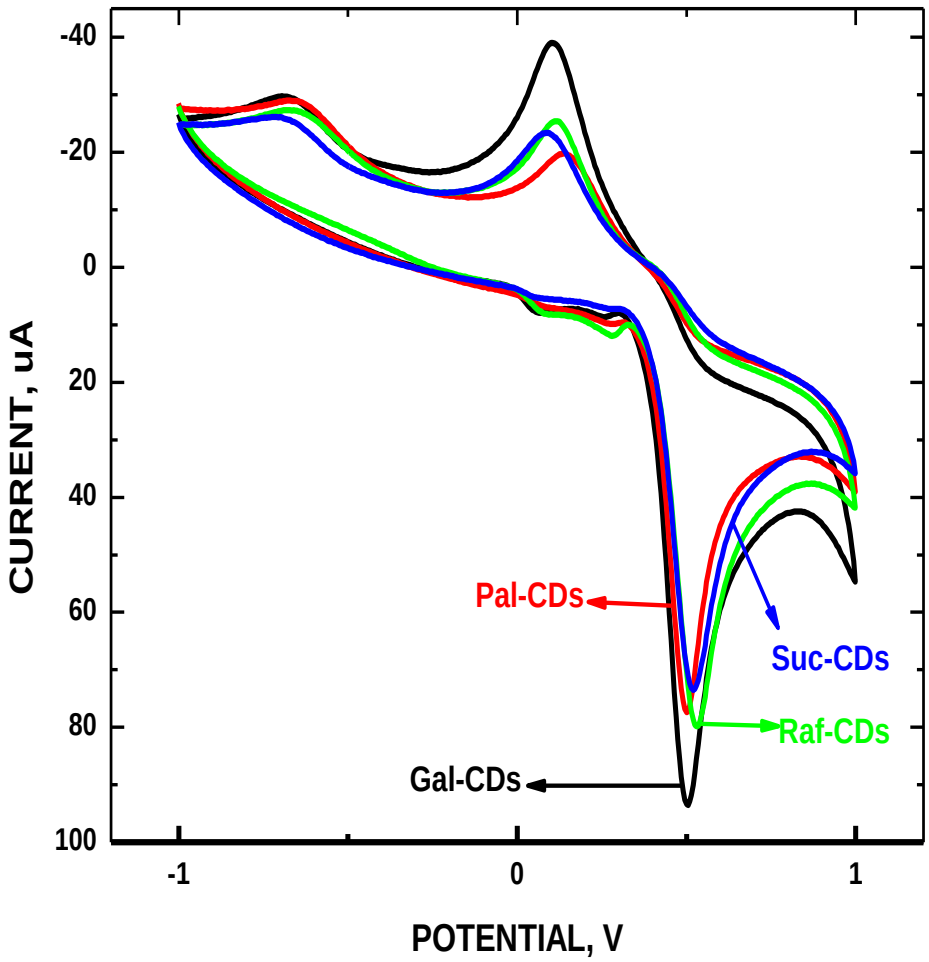

Fig 37. CVs of different saccharides based CD in 1 mM APAP.

The oxidation of acetaminophen (APAP) occurs at a potential close to 0.5 V. Among various carbon materials, sucrose exhibits the highest graphene defect density, and it demonstrates the lowest electrochemical sensitivity for APAP sensing. This result absolutely aligen with the literature Chusuei et al [43]. Suc-CDs, Pal-CDs, Gla-CDs, Raf-CDs, I_D/I_G = 0.195, I_D/I_G = 0.117, I_D/I_G =0.0982 [Chusuei et.al 2021 Electroanalysis], and I_D/I_G = 0.0976 respectively. In this context, the Raf-CDs exhibit the lowest defect density, albeit marginally lower than that of Gal-CDs. Surprisingly, despite the conventional hypothesis proposed by Chusuei et al., which suggests that a lower defect density enhances electron transfer rate, the electrochemical sensing results for acetaminophen (APAP)

indicate that Gal-CDs outperform Raf-CDs. This discrepancy challenges the anticipated relationship between defect density and electron transfer rate when the redox potential falls outside the range of -2 to +3 V, where the density of states is significantly distant from the Fermi level. But all other results are in agreement with the hypothesis purposed by Chusuei et al.

The correlation of graphene defects density with the electrochemical sensing of APAP is illustrated as

Defects density decreasing

Suc-CD

Pal-CD

Gal-CD

Raf-CD

electrochemical sensitivity

Gal-CD

Raf-CD

Pal-CD

Suc-CD

Electrochemical sensing of HVA

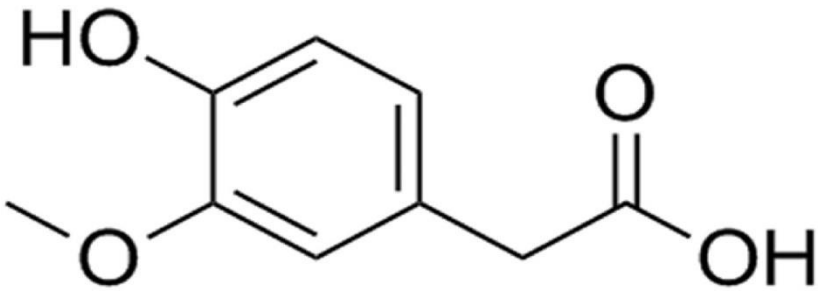

Fig 38. Homovanilic Acid molecule

The electrochemical detection of homovanilic acid (HVA) was attempted using saccharide-based carbon dots. A solution of 4.6 mg HVA in 25 ml phosphate buffer at pH 7 resulted in a 1 mM concentration. The working electrode, a glassy carbon electrode, incorporated various saccharide-based carbon dots and Nafion as an encapsulating agent. Cyclic voltammetry (CV) was conducted within a potential range of -1 to +1 V. An anodic peak current of approximately 20 µA was observed at a potential of 0.5 V for the 1 mM HVA solution. Interestingly, the peak current did not exhibit an increase with the rising concentration of HVA.

Appendix C - Permissions

Permission for Figure 1: No special permission is required to reuse all or part of article published by MDPI, including figures and tables. For articles published under an open access Creative Common CC BY license, any part of the article may be reused without permission provided that the original article is clearly cited. Reuse of an article does not imply endorsement by the authors or MDPI.

Permission for Figure 2
Structural Defects in Graphene
Author:
Florian Banhart, Jani Kotakoski, Arkady V. Krasheninnikov
Publication:
ACS Nano
Publisher:
American Chemical Society
Date:
Jan 1, 2011
Copyright © 2011, American Chemical Society

PERMISSION/LICENSE IS GRANTED FOR YOUR ORDER AT NO CHARGE

Permission for Figure 3:
Open access

Permission for Figure 4:


Intense Raman D Band without Disorder in Flattened Carbon Nanotubes

Author:

Emmanuel Picheau, Anthony Impellizzeri, Dmitry Rybkovskiy, et al

Publication:

ACS Nano

Publisher:

American Chemical Society

Date: Jan 1, 2021

Permission for Figure 5:

Permission for Figure 6:

Permission for Figure 7: